Searches for Neutral Higgs Bosons in e^+e^- Collisions around $\sqrt{s} = 189$ GeV

P. Abreu, W. Adam, T. Adye, P. Adzic, Z. Albrecht, T. Alderweireld, G D. Alekseev, R. Alemany, T. Allmendinger, P P. Allport, et al.

EUROPEAN ORGANIZATION FOR NUCLEAR RESEARCH

CERN–EP-2000-038

10 March 2000

Searches for Neutral Higgs Bosons in e^+e^- Collisions around $\sqrt{s} = 189$ GeV

DELPHI Collaboration

Abstract

Searches for neutral Higgs bosons in the Standard Model and the MSSM have been performed using data collected by the DELPHI experiment at a centre-of-mass energy of 188.7 GeV, corresponding to an integrated luminosity of 158 pb^{-1}. These analyses are used, in combination with our results from lower energies, to set new 95% confidence level lower mass bounds on the Standard Model Higgs boson (94.6 GeV/c^2) and on the lightest neutral scalar (82.6 GeV/c^2) and neutral pseudoscalar (84.1 GeV/c^2) Higgs bosons in a representative scan of the MSSM parameters. The results are also interpreted in the framework of a general two-Higgs doublet model.

(Accepted by E. Phys. J. C)

P.Abreu[22], W.Adam[52], T.Adye[38], P.Adzic[12], Z.Albrecht[18], T.Alderweireld[2], G.D.Alekseev[17], R.Alemany[51], T.Allmendinger[18], P.P.Allport[23], S.Almehed[25], U.Amaldi[29], N.Amapane[47], S.Amato[49], E.G.Anassontzis[3], P.Andersson[46], A.Andreazza[9], S.Andringa[22], P.Antilogus[26], W-D.Apel[18], Y.Arnoud[9], B.Åsman[46], J-E.Augustin[26], A.Augustinus[9], P.Baillon[9], P.Bambade[20], F.Barao[22], G.Barbiellini[48], R.Barbier[26], D.Y.Bardin[17], G.Barker[18], A.Baroncelli[40], M.Battaglia[16], M.Baubillier[24], K-H.Becks[54], M.Begalli[6], A.Behrmann[54], P.Beilliere[8], Yu.Belokopytov[9], K.Belous[44], N.C.Benekos[33], A.C.Benvenuti[5], C.Berat[15], M.Berggren[26], D.Bertini[26], D.Bertrand[2], M.Besancon[41], M.Bigi[47], M.S.Bilenky[17], M-A.Bizouard[20], D.Bloch[10], H.M.Blom[32], M.Bonesini[29], W.Bonivento[28], M.Boonekamp[41], P.S.L.Booth[23], A.W.Borgland[4], G.Borisov[20], C.Bosio[43], O.Botner[50], E.Boudinov[32], B.Bouquet[20], C.Bourdarios[20], T.J.V.Bowcock[23], I.Boyko[17], I.Bozovic[12], M.Bozzo[14], M.Bracko[45], P.Branchini[40], R.A.Brenner[50], P.Bruckman[9], J-M.Brunet[8], L.Bugge[34], T.Buran[34], B.Buschbeck[52], P.Buschmann[54], S.Cabrera[51], M.Caccia[28], M.Calvi[29], T.Camporesi[9], V.Canale[39], F.Carena[9], L.Carroll[23], C.Caso[14], M.V.Castillo Gimenez[51], A.Cattai[9], F.R.Cavallo[5], V.Chabaud[9], M.Chapkin[44], Ph.Charpentier[9], L.Chaussard[26], P.Checchia[37], G.A.Chelkov[17], R.Chierici[47], P.Chliapnikov[9,44], P.Chochula[7], V.Chorowicz[26], J.Chudoba[31], K.Cieslik[19], P.Collins[9], R.Contri[14], E.Cortina[51], G.Cosme[20], F.Cossutti[9], H.B.Crawley[1], D.Crennell[38], S.Crepe[15], G.Crosetti[14], J.Cuevas Maestro[35], S.Czellar[16], M.Davenport[9], W.Da Silva[24], G.Della Ricca[48], P.Delpierre[27], N.Demaria[9], A.De Angelis[48], W.De Boer[18], C.De Clercq[2], B.De Lotto[48], A.De Min[37], L.De Paula[49], H.Dijkstra[9], L.Di Ciaccio[9,39], J.Dolbeau[8], K.Doroba[53], M.Dracos[10], J.Drees[54], M.Dris[33], A.Duperrin[26], J-D.Durand[9], G.Eigen[4], T.Ekelof[50], G.Ekspong[46], M.Ellert[50], M.Elsing[9], J-P.Engel[10], M.Espirito Santo[22], G.Fanourakis[12], D.Fassouliotis[12], J.Fayot[24], M.Feindt[18], P.Ferrari[28], A.Ferrer[51], E.Ferrer-Ribas[20], F.Ferro[14], S.Fichet[24], A.Firestone[1], U.Flagmeyer[54], H.Foeth[9], E.Fokitis[33], F.Fontanelli[14], B.Franek[38], A.G.Frodesen[4], R.Fruhwirth[52], F.Fulda-Quenzer[20], J.Fuster[51], A.Galloni[23], D.Gamba[47], S.Gamblin[20], M.Gandelman[49], C.Garcia[51], C.Gaspar[9], M.Gaspar[49], U.Gasparini[37], Ph.Gavillet[9], E.N.Gazis[33], D.Gele[10], N.Ghodbane[26], I.Gil[51], F.Glege[54], R.Gokieli[9,53], B.Golob[9,45], G.Gomez-Ceballos[42], P.Goncalves[22], I.Gonzalez Caballero[42], G.Gopal[38], L.Gorn[1], Yu.Gouz[44], V.Gracco[14], J.Grahl[1], E.Graziani[40], P.Gris[41], G.Grosdidier[20], K.Grzelak[53], J.Guy[38], F.Hahn[9], S.Hahn[54], S.Haider[9], A.Hallgren[50], K.Hamacher[54], J.Hansen[34], F.J.Harris[36], V.Hedberg[9,25], S.Heising[18], J.J.Hernandez[51], P.Herquet[2], H.Herr[9], T.L.Hessing[36], J.-M.Heuser[54], E.Higon[51], S-O.Holmgren[46], P.J.Holt[36], S.Hoorelbeke[2], M.Houlden[23], J.Hrubec[52], M.Huber[18], K.Huet[2], G.J.Hughes[23], K.Hultqvist[9,46], J.N.Jackson[23], R.Jacobsson[9], P.Jalocha[19], R.Janik[7], Ch.Jarlskog[25], G.Jarlskog[25], P.Jarry[41], B.Jean-Marie[20], D.Jeans[36], E.K.Johansson[46], P.Jonsson[26], C.Joram[9], P.Juillot[10], L.Jungermann[18], F.Kapusta[24], K.Karafasoulis[12], S.Katsanevas[26], E.C.Katsoufis[33], R.Keranen[18], G.Kernel[45], B.P.Kersevan[45], Yu.Khokhlov[44], B.A.Khomenko[17], N.N.Khovanski[17], A.Kiiskinen[16], B.King[23], A.Kinvig[23], N.J.Kjaer[9], O.Klapp[54], H.Klein[9], P.Kluit[32], P.Kokkinias[12], V.Kostioukhine[44], C.Kourkoumelis[3], O.Kouznetsov[41], M.Krammer[52], E.Kriznic[45], Z.Krumstein[17], P.Kubinec[7], J.Kurowska[53], K.Kurvinen[16], J.W.Lamsa[1], D.W.Lane[1], V.Lapin[44], J-P.Laugier[41], R.Lauhakangas[16], G.Leder[52], F.Ledroit[15], V.Lefebure[2], L.Leinonen[46], A.Leisos[12], R.Leitner[31], J.Lemonne[2], G.Lenzen[54], V.Lepeltier[20], T.Lesiak[19], M.Lethuillier[41], J.Libby[36], W.Liebig[54], D.Liko[9], A.Lipniacka[9,46], I.Lippi[37], B.Loerstad[25], J.G.Loken[36], J.H.Lopes[49], J.M.Lopez[42], R.Lopez-Fernandez[15], D.Loukas[12], P.Lutz[41], L.Lyons[36], J.MacNaughton[52], J.R.Mahon[6], A.Maio[22], A.Malek[54], T.G.M.Malmgren[46], S.Maltezos[33], V.Malychev[17], F.Mandl[52], J.Marco[42], R.Marco[42], B.Marechal[49], M.Margoni[37], J-C.Marin[9], C.Mariotti[9], A.Markou[12], C.Martinez-Rivero[20], F.Martinez-Vidal[51], S.Marti i Garcia[9], J.Masik[13], N.Mastroyiannopoulos[12], F.Matorras[42], C.Matteuzzi[29], G.Matthiae[39], F.Mazzucato[37], M.Mazzucato[37], M.Mc Cubbin[23], R.Mc Kay[1], R.Mc Nulty[23], G.Mc Pherson[23], C.Meroni[28], W.T.Meyer[1], A.Miagkov[44], E.Migliore[9], L.Mirabito[26], W.A.Mitaroff[52], U.Mjoernmark[25], T.Moa[46], M.Moch[18], R.Moeller[30], K.Moenig[9,11], M.R.Monge[14], X.Moreau[24], P.Morettini[14], G.Morton[36], U.Mueller[54], K.Muenich[54], M.Mulders[32], C.Mulet-Marquis[15], R.Muresan[25], W.J.Murray[38], B.Muryn[19], G.Myatt[36], T.Myklebust[34], F.Naraghi[15], M.Nassiakou[12], F.L.Navarria[5], S.Navas[51], K.Nawrocki[53], P.Negri[29], N.Neufeld[9], R.Nicolaidou[41], B.S.Nielsen[30], P.Niezurawski[53], M.Nikolenko[10,17], V.Nomokonov[16], A.Nygren[25], V.Obraztsov[44], A.G.Olshevski[17], A.Onofre[22], R.Orava[16], G.Orazi[10], K.Osterberg[16], A.Ouraou[41], M.Paganoni[29], S.Paiano[5], R.Pain[24], R.Paiva[22], J.Palacios[36], H.Palka[19], Th.D.Papadopoulou[9,33], K.Papageorgiou[12], L.Pape[9], C.Parkes[9], F.Parodi[14], U.Parzefall[23], A.Passeri[40], O.Passon[54], T.Pavel[25], M.Pegoraro[37], L.Peralta[22], M.Pernicka[52], A.Perrotta[5], C.Petridou[48], A.Petrolini[14], H.T.Phillips[38], F.Pierre[41], M.Pimenta[22], E.Piotto[28], T.Podobnik[45], M.E.Pol[6], G.Polok[19], P.Poropat[48], V.Pozdniakov[17], P.Privitera[39], N.Pukhaeva[17], A.Pullia[29], D.Radojicic[36], S.Ragazzi[29], H.Rahmani[33], J.Rames[13], P.N.Ratoff[21], A.L.Read[34], P.Rebecchi[9], N.G.Redaelli[29], M.Regler[52], J.Rehn[18], D.Reid[32], R.Reinhardt[54], P.B.Renton[36], L.K.Resvanis[3], F.Richard[20], J.Ridky[13], G.Rinaudo[47], I.Ripp-Baudot[10], O.Rohne[34], A.Romero[47], P.Ronchese[37], E.I.Rosenberg[1], P.Rosinsky[7], P.Roudeau[20], T.Rovelli[5], Ch.Royon[41], V.Ruhlmann-Kleider[41], A.Ruiz[42], H.Saarikko[16], Y.Sacquin[41], A.Sadovsky[17], G.Sajot[15], J.Salt[51], D.Sampsonidis[12], M.Sannino[14], Ph.Schwemling[24], B.Schwering[54], U.Schwickerath[18], F.Scuri[48], P.Seager[21], Y.Sedykh[17], A.M.Segar[36], N.Seibert[18], R.Sekulin[38], R.C.Shellard[6], M.Siebel[54], L.Simard[41], F.Simonetto[37], A.N.Sisakian[17], G.Smadja[26], O.Smirnova[25], G.R.Smith[38], O.Solovianov[44], A.Sopczak[18], R.Sosnowski[53], T.Spassov[22], E.Spiriti[40], S.Squarcia[14], C.Stanescu[40], S.Stanic[45], M.Stanitzki[18], K.Stevenson[36], A.Stocchi[20], J.Strauss[52], R.Strub[10], B.Stugu[4], M.Szczekowski[53], M.Szeptycka[53], T.Tabarelli[29], A.Taffard[23], F.Tegenfeldt[50], F.Terranova[29], J.Thomas[36], J.Timmermans[32], N.Tinti[5], L.G.Tkatchev[17], M.Tobin[23], S.Todorova[10], A.Tomaradze[2], B.Tome[22], A.Tonazzo[9], L.Tortora[40], P.Tortosa[51], G.Transtromer[25], D.Treille[9], G.Tristram[8],

M.Trochimczuk[53], C.Troncon[28], M-L.Turluer[41], I.A.Tyapkin[17], S.Tzamarias[12], O.Ullaland[9], V.Uvarov[44], G.Valenti[9,5], E.Vallazza[48], C.Vander Velde[2], P.Van Dam[32], W.Van den Boeck[2], W.K.Van Doninck[2], J.Van Eldik[9,32], A.Van Lysebetten[2], N.van Remortel[2], I.Van Vulpen[32], G.Vegni[28], L.Ventura[37], W.Venus[38,9], F.Verbeure[2], M.Verlato[37], L.S.Vertogradov[17], V.Verzi[39], D.Vilanova[41], L.Vitale[48], E.Vlasov[44], A.S.Vodopyanov[17], G.Voulgaris[3], V.Vrba[13], H.Wahlen[54], C.Walck[46], A.J.Washbrook[23], C.Weiser[9], D.Wicke[54], J.H.Wickens[2], G.R.Wilkinson[36], M.Winter[10], M.Witek[19], G.Wolf[9], J.Yi[1], O.Yushchenko[44], A.Zalewska[19], P.Zalewski[53], D.Zavrtanik[45], E.Zevgolatakos[12], N.I.Zimin[17,25], A.Zintchenko[17], Ph.Zoller[10], G.C.Zucchelli[46], G.Zumerle[37]

[1] Department of Physics and Astronomy, Iowa State University, Ames IA 50011-3160, USA
[2] Physics Department, Univ. Instelling Antwerpen, Universiteitsplein 1, B-2610 Antwerpen, Belgium
and IIHE, ULB-VUB, Pleinlaan 2, B-1050 Brussels, Belgium
and Faculté des Sciences, Univ. de l'Etat Mons, Av. Maistriau 19, B-7000 Mons, Belgium
[3] Physics Laboratory, University of Athens, Solonos Str. 104, GR-10680 Athens, Greece
[4] Department of Physics, University of Bergen, Allégaten 55, NO-5007 Bergen, Norway
[5] Dipartimento di Fisica, Università di Bologna and INFN, Via Irnerio 46, IT-40126 Bologna, Italy
[6] Centro Brasileiro de Pesquisas Físicas, rua Xavier Sigaud 150, BR-22290 Rio de Janeiro, Brazil
and Depto. de Física, Pont. Univ. Católica, C.P. 38071 BR-22453 Rio de Janeiro, Brazil
and Inst. de Física, Univ. Estadual do Rio de Janeiro, rua São Francisco Xavier 524, Rio de Janeiro, Brazil
[7] Comenius University, Faculty of Mathematics and Physics, Mlynska Dolina, SK-84215 Bratislava, Slovakia
[8] Collège de France, Lab. de Physique Corpusculaire, IN2P3-CNRS, FR-75231 Paris Cedex 05, France
[9] CERN, CH-1211 Geneva 23, Switzerland
[10] Institut de Recherches Subatomiques, IN2P3 - CNRS/ULP - BP20, FR-67037 Strasbourg Cedex, France
[11] Now at DESY-Zeuthen, Platanenallee 6, D-15735 Zeuthen, Germany
[12] Institute of Nuclear Physics, N.C.S.R. Demokritos, P.O. Box 60228, GR-15310 Athens, Greece
[13] FZU, Inst. of Phys. of the C.A.S. High Energy Physics Division, Na Slovance 2, CZ-180 40, Praha 8, Czech Republic
[14] Dipartimento di Fisica, Università di Genova and INFN, Via Dodecaneso 33, IT-16146 Genova, Italy
[15] Institut des Sciences Nucléaires, IN2P3-CNRS, Université de Grenoble 1, FR-38026 Grenoble Cedex, France
[16] Helsinki Institute of Physics, HIP, P.O. Box 9, FI-00014 Helsinki, Finland
[17] Joint Institute for Nuclear Research, Dubna, Head Post Office, P.O. Box 79, RU-101 000 Moscow, Russian Federation
[18] Institut für Experimentelle Kernphysik, Universität Karlsruhe, Postfach 6980, DE-76128 Karlsruhe, Germany
[19] Institute of Nuclear Physics and University of Mining and Metalurgy, Ul. Kawiory 26a, PL-30055 Krakow, Poland
[20] Université de Paris-Sud, Lab. de l'Accélérateur Linéaire, IN2P3-CNRS, Bât. 200, FR-91405 Orsay Cedex, France
[21] School of Physics and Chemistry, University of Lancaster, Lancaster LA1 4YB, UK
[22] LIP, IST, FCUL - Av. Elias Garcia, 14-1^{o}, PT-1000 Lisboa Codex, Portugal
[23] Department of Physics, University of Liverpool, P.O. Box 147, Liverpool L69 3BX, UK
[24] LPNHE, IN2P3-CNRS, Univ. Paris VI et VII, Tour 33 (RdC), 4 place Jussieu, FR-75252 Paris Cedex 05, France
[25] Department of Physics, University of Lund, Sölvegatan 14, SE-223 63 Lund, Sweden
[26] Université Claude Bernard de Lyon, IPNL, IN2P3-CNRS, FR-69622 Villeurbanne Cedex, France
[27] Univ. d'Aix - Marseille II - CPP, IN2P3-CNRS, FR-13288 Marseille Cedex 09, France
[28] Dipartimento di Fisica, Università di Milano and INFN, Via Celoria 16, IT-20133 Milan, Italy
[29] Università degli Studi di Milano - Bicocca, Via Emanuelli 15, IT-20126 Milan, Italy
[30] Niels Bohr Institute, Blegdamsvej 17, DK-2100 Copenhagen Ø, Denmark
[31] IPNP of MFF, Charles Univ., Areal MFF, V Holesovickach 2, CZ-180 00, Praha 8, Czech Republic
[32] NIKHEF, Postbus 41882, NL-1009 DB Amsterdam, The Netherlands
[33] National Technical University, Physics Department, Zografou Campus, GR-15773 Athens, Greece
[34] Physics Department, University of Oslo, Blindern, NO-1000 Oslo 3, Norway
[35] Dpto. Fisica, Univ. Oviedo, Avda. Calvo Sotelo s/n, ES-33007 Oviedo, Spain
[36] Department of Physics, University of Oxford, Keble Road, Oxford OX1 3RH, UK
[37] Dipartimento di Fisica, Università di Padova and INFN, Via Marzolo 8, IT-35131 Padua, Italy
[38] Rutherford Appleton Laboratory, Chilton, Didcot OX11 OQX, UK
[39] Dipartimento di Fisica, Università di Roma II and INFN, Tor Vergata, IT-00173 Rome, Italy
[40] Dipartimento di Fisica, Università di Roma III and INFN, Via della Vasca Navale 84, IT-00146 Rome, Italy
[41] DAPNIA/Service de Physique des Particules, CEA-Saclay, FR-91191 Gif-sur-Yvette Cedex, France
[42] Instituto de Fisica de Cantabria (CSIC-UC), Avda. los Castros s/n, ES-39006 Santander, Spain
[43] Dipartimento di Fisica, Università degli Studi di Roma La Sapienza, Piazzale Aldo Moro 2, IT-00185 Rome, Italy
[44] Inst. for High Energy Physics, Serpukov P.O. Box 35, Protvino, (Moscow Region), Russian Federation
[45] J. Stefan Institute, Jamova 39, SI-1000 Ljubljana, Slovenia and Laboratory for Astroparticle Physics,
Nova Gorica Polytechnic, Kostanjeviska 16a, SI-5000 Nova Gorica, Slovenia,
and Department of Physics, University of Ljubljana, SI-1000 Ljubljana, Slovenia
[46] Fysikum, Stockholm University, Box 6730, SE-113 85 Stockholm, Sweden
[47] Dipartimento di Fisica Sperimentale, Università di Torino and INFN, Via P. Giuria 1, IT-10125 Turin, Italy
[48] Dipartimento di Fisica, Università di Trieste and INFN, Via A. Valerio 2, IT-34127 Trieste, Italy
and Istituto di Fisica, Università di Udine, IT-33100 Udine, Italy
[49] Univ. Federal do Rio de Janeiro, C.P. 68528 Cidade Univ., Ilha do Fundão BR-21945-970 Rio de Janeiro, Brazil
[50] Department of Radiation Sciences, University of Uppsala, P.O. Box 535, SE-751 21 Uppsala, Sweden
[51] IFIC, Valencia-CSIC, and D.F.A.M.N., U. de Valencia, Avda. Dr. Moliner 50, ES-46100 Burjassot (Valencia), Spain
[52] Institut für Hochenergiephysik, Österr. Akad. d. Wissensch., Nikolsdorfergasse 18, AT-1050 Vienna, Austria
[53] Inst. Nuclear Studies and University of Warsaw, Ul. Hoza 69, PL-00681 Warsaw, Poland
[54] Fachbereich Physik, University of Wuppertal, Postfach 100 127, DE-42097 Wuppertal, Germany

1 Introduction

In the framework of the Standard Model (SM) there is one physical Higgs boson, H, which is a neutral CP-even scalar. At LEP II the most likely production process is through the s-channel, $e^+e^- \rightarrow Z^* \rightarrow HZ$. The W^+W^- and ZZ fusion t-channel production processes in some of the channels described below are not considered here, but their contribution is typically below 10% in the range of masses considered in this study.

The results of the search for the SM Higgs are also interpreted in terms of the lightest scalar Higgs boson, h, in the Minimal Super-symmetric Standard Model (MSSM). This model predicts also a CP-odd pseudo-scalar, A, produced mostly in the $e^+e^- \rightarrow hA$ process at LEP II. This associated production is also considered in this paper.

With the data taken previously at $\sqrt{s}$= 183 GeV DELPHI excluded a SM Higgs boson with mass less than 85.7 GeV/c^2 [1], and set limits on h and A of the MSSM of 74.4 GeV/c^2 and 75.3 GeV/c^2 respectively. The present analyses therefore concentrate on masses between these and the kinematic limit. Note that the LEP Higgs working group [2] has found mass limits of 89.7 GeV/c^2 for H, 80.1 GeV/c^2 for h and 80.6 GeV/c^2 for A, under assumptions generally referred to as the benchmark scan, when combining the data of the four LEP experiments from data taken up to 183 GeV.

In the HZ channel, all known decays of the Z boson have been taken into account (hadrons, charged leptons and neutrinos) while the analyses have been optimised either for decays of the Higgs into $b\bar{b}$, making use of the expected high branching fraction of this mode, or for Higgs boson decays into a pair of τ's. A dedicated search for the invisible Higgs boson decay modes will be reported separately. The hA production has been searched for in the 4b and $b\bar{b}$ $\tau^+\tau^-$ channels.

There are separate analyses for the different decay modes of the Higgs and Z bosons. Some common features are discussed in Sect. 3, the $H\mu^+\mu^-$ and He^+e^- channels in Sect. 4, channels involving jets and τ's in Sect. 5 and $H\nu\bar{\nu}$ in Sect. 6. Purely hadronic final states are discussed in Sect. 7. The results are presented in Sect. 8.

2 Data samples overview and the DELPHI detector

For most of the data collected in 1998, LEP was running at energies around 189 GeV. DELPHI recorded an integrated luminosity of (158$\pm$1) pb^{-1} at a mean energy of 188.7 GeV.

Large numbers of background and signal events have been produced by Monte Carlo simulation using the DELPHI detector simulation program [3]. The size of these samples is typically about 100 times the luminosity of the collected data. Background was generated with `PYTHIA` [4] and `KORALZ` [5] for ($e^+e^- \rightarrow f\bar{f}\,\gamma$), `PYTHIA` and `EXCALIBUR` [6] for the four-fermion background and `TWOGAM` [7] and `BDK` [8] for two-photon processes. `BABAMC` [9] was used to simulate Bhabha events in the main acceptance region.

Signal events were produced using the `HZHA` [10] generator. For the SM process the Higgs mass was varied in 5 GeV/c^2 steps from 70 GeV/c^2 to 100 GeV/c^2, while for hA , the A mass was varied between 70 and 90 GeV/c^2 with $\tan\beta$ (the ratio of the vacuum expectation values of the two doublets) either 2 or 20. This fixes the h mass, almost equal to m_A for $\tan\beta = 20$ and significantly lower than m_A if $\tan\beta = 2$.

The HZ simulated samples were classified according to the Higgs and Z boson decay modes. For He^+e^-, $H\mu^+\mu^-$ and $H\nu\bar{\nu}$ the natural SM mix of H decay modes was permitted. In the $Hq\bar{q}$ channel the $\tau\tau$ decay mode was removed, and we generated separately the two channels involving τ leptons for which one of the bosons is forced to decay to τ's and

the other hadronically. Finally, for the hA simulations final states involving either four b quarks or two b quarks and two τ's were simulated. Efficiencies were defined relative to these states. The size of these samples varied from 2000 to 20,000 events.

The detector was unchanged from the previous data taking period. Thus we refer to our previous publication [1] for a short description. More details can be found in references [3,11].

3 Common features for all channels

3.1 Particle selection

In all analyses, charged particles are selected if their momentum is greater than 100 MeV/c and if they originate from the interaction region (within 10 cm along the beam direction and within 4 cm in the transverse plane). Neutral particles are defined either as energy clusters in the calorimeters not associated to charged particle tracks, or as reconstructed vertices of photon conversions, interactions of neutral hadrons or decays of neutral particles in the tracking volume. All neutral clusters of energy greater than 200 MeV (electromagnetic) or 500 MeV (hadronic) are used; clusters in the range 100-500 MeV are considered with specific quality criteria in some analyses. The $\pi^{\pm}$ mass is used for all charged particles except identified leptons, while zero mass is used for electromagnetic clusters and the K^0 mass is assigned to neutral hadronic clusters.

3.2 b-quark identification

The method of separation of b quarks from other flavours is described in [12], where the various differences between B-hadrons and other particles are accumulated in a single variable, hereafter denoted x_{b} for an event and x_{b}^i for jet i. A major input to the combined variable is the probability that all tracks in a group originate from the interaction point. x_{b} combines this probability with information from secondary vertices (the mass computed from the particles assigned to the secondary vertex, the rapidity of those particles, and the fraction of the jet momentum carried by them) and also the transverse momentum (with respect to its jet axis) of the leptons, using the likelihood ratio technique. Increasing values of x_{b} correspond to increasingly 'b-like' events (or jets).

The procedure is calibrated on events recorded in the same experimental conditions at the Z resonance. The performance of the combined b-tagging is described in Ref. [13], and the impact parameter tagging in Ref. [14]. The overall performance is illustrated in Figure 1.

A careful study of possible systematic effects, including data versus simulation agreement at the Z pole (checked inclusively, per flavour and for multi-jet events), leads to an overall relative b-tagging uncertainty below 5%, varying slightly with the exact tagging value used. At high energy, an inclusive comparison of data with simulation confirms this number. The gluon splitting rates into $\mathrm{b\bar{b}}$ and $\mathrm{c\bar{c}}$ have been rescaled in the simulation according to the DELPHI [15] measurement. In addition, a 50% uncertainty on these splitting rates is applied to the $\mathrm{q\bar{q}}$ (γ) background estimate.

3.3 Constrained fits

In most channels a constrained fit [16] is performed to extract the Higgs mass, and often to reject background processes as well. If only total energy and momentum conservation

are imposed then the fit is referred to as '4-C', while some fits require the Z mass as well, either as a fixed value, or taking into account the Breit–Wigner shape of the Z resonance. In both cases such fits are referred to as '5-C'. In order to allow the removal of most of the radiative return to the Zevents, an algorithm has been developed [17] in order to estimate the effective energy of the e^+e^- collision. This algorithm makes use of a '3-C' kinematic fit in order to test the presence of an initial state photon parallel to the beam direction and then lost in the beam pipe. This effective centre-of-mass energy is called $\sqrt{s'}$ throughout the paper.

3.4 Confidence level calculations

The procedure used to compute the confidence levels is the same as that used in our previous publications [1,18] but the discriminant information is now two-dimensional: the first variable used is the reconstructed mass, the second one is either the x_b (for the electron and muon channels) or the likelihood (for all other channels). As far as the mass information is concerned, the reconstructed Higgs boson mass is used in the hZ channels and the sum of the reconstructed h and A masses in the hA channels (for the pairing with minimal mass difference in the four-jet channel). In order to make full use of the information contained in the second variable the selections are looser than in the past: the method used for deriving the confidence levels ensures that adding regions of lower signal and higher background can only enhance the performance expected from a tighter selection. Since the distributions, represented as two-dimensional histograms, are derived from simulation samples, the limited statistics in some bins are a potential problem: statistical fluctuations can artificially increase the expected sensitivity. This possible systematic shift of the confidence level has been estimated comparing the expected results using the full simulation sample with those derived from fractions of this sample. The bin sizes were carefully chosen to keep full sensitivity while avoiding any significant bias caused by this effect.

4 Higgs boson searches in events with jets and electrons or muons

4.1 Electron channel

The analysis follows what has already been published [1], with the following improvements in the selection cuts. To reinforce the Bhabha veto, the preselection described in [1] has been complemented by a rejection of electron candidate pairs having acoplanarity (defined as the supplement of the angle between the transverse momenta of the two electrons) below 3 degrees and energies above 40 GeV. To allow for the tau decays of the Higgs boson while keeping a good purity, the requirement on the minimum event charged multiplicity has been raised to 8 except if the recoiling system from the electron candidate pair is made of two jets, each with a charged multiplicity lower than or equal to 3 and with a mass below 2 GeV/c^2. This defines the preselection.

The energy of the slower/faster electron is required to be above 15/20 GeV. Electron isolation angles with respect to the closest jet are required to be more than 20° for the most isolated electron and more than 8° for the other. Global kinematic fits [16] are performed, imposing total energy and momentum conservation and constraining the invariant mass of the e^+e^- system to m_Z (5-C fits). If the fit probability is below 10^{-8}, the

fit procedure is redone for fixed values of the e^+e^- mass between 36.5 and 105 GeV/c^2, in order to allow for the tails of the Z mass distribution. For each mass a combined probability is determined as the product of the χ^2 probability times the Breit-Wigner probability for the Z mass, and the mass giving the maximum combined probability is retained. Events with a combined probability below 10^{-8} are rejected. As the search is restricted to high mass Higgs bosons produced in association with a Z particle, the sum of the masses of the electron pair and of the recoiling system as given by the kinematic fit is required to be above 150 GeV/c^2 and the difference in the range from -100 GeV/c^2 to 50 GeV/c^2. The fitted recoil mass and the global b-tagging variable x_b are used for the two-dimensional calculation of the confidence levels.

Table 1 shows the effect of the cuts on data, simulated background and signal events. The agreement between data and background simulation is illustrated at preselection level in Figure 2 which shows the distributions of the main analysis variables, namely, the slow electron energy, the fitted mass of the jet system, the minimum electron isolation angle and the global event b-tagging variable x_{b}.

The final background amounts to $6.63 \pm 0.26\ (stat.)^{+0.59}_{-0.93}\ (syst.)$ events, and is mainly due to $e^+e^-q\bar{q}$ (ZZ) events. Illustrations of the two-dimensional distribution, used as input for the confidence level computations are shown in figure 3 for data, simulated background and signal events (for m_{H} =95 GeV/c^2). Table 2 shows the selection efficiency for different Higgs boson masses. The systematic uncertainties have been evaluated as described in [1]. Among the events selected in data, one has a high x_b value and thus is kept in the final mass-plot, for which the supplementary cut $x_b > -1.8$ was applied.

4.2 Muon channel

The analysis is based upon the same discriminant variables as in [1], but the selection criteria have been re-optimised, as explained in [1], to afford the best sensitivity to the expected signal at 188.7 GeV. The preselection remains unchanged except that events must now have at least nine charged particle tracks. Two muons are required with opposite charges, momenta greater than 34 GeV/c and 19 GeV/c, and an opening angle larger than 10°. The muon isolation angle with respect to the closer jet must be greater than 16° for the most isolated muon and greater than 8° for the other one. A 5-C kinematic fit is then performed to test the compatibility of the di-muon mass with the Z mass. Events are kept only if the fit converges. The fitted recoiling mass is chosen as the first discriminant variable for the two-dimensional calculation of the confidence levels. The second variable is the global b-quark variable x_{b}.

Table 1 details the effect of the selections on data and simulated samples of background and signal events. The agreement of simulation with data is good. This can also be seen in Figure 4, which shows the total energy of the charged particles, the momentum of the fast muon candidate and the content in b-quark of the event after the preselection. The isolation of the muons with respect to the closest jet is also given after the lepton pair selection. At the end of the analysis, 5 events are selected in the data in good agreement with the expected background of $5.09 \pm 0.19(stat.) \pm 0.21(syst.)$ events coming mainly from ZZ. Finally the signal efficiencies for different Higgs boson masses are given in Table 2. The systematic uncertainties on background and efficiencies have been derived as explained in [1]. The two events with the largest values of x_{b} are kept for the final mass-plot.

5 Higgs boson searches in events with jets and taus

Three channels are covered by this analysis, two for the SM, depending of which boson decays into $\tau^+\tau^-$, and one for the MSSM. Hadronic events are selected by requiring at least ten charged particles, a total reconstructed energy greater than $0.4\sqrt{s}$, a reconstructed charged energy above $0.2\sqrt{s}$ and an effective centre-of-mass energy, $\sqrt{s'}$, greater than 120 GeV. This defines the preselection.

A search for τ lepton candidates is then performed using a likelihood technique. Clusters of one or three charged particles are first preselected if they are isolated from all other particles by more than 10°, if the cluster momentum is above 2 GeV/c and if all particles in a 10° cone around the cluster direction make an invariant mass below 2 GeV/c^2. The likelihood variable is calculated for the preselected clusters using distributions of the cluster momentum, of its isolation angle and of the probability that the tracks forming the cluster come from the primary vertex. Pairs of τ candidates with opposite charges and an opening angle of at least 90° are selected using a cut on the product of their likelihoods, considering both the 1-1 (where the two τ leptons decay to one prong) and 1-3 (with at least one τ decaying to three prongs) topologies. As an example, Figure 5a shows the τ selection likelihood distribution for the selected events in the 1-1 topology.

Two slim jets are then reconstructed with all particles (charged and neutral) inside a 10° cone around the cluster directions. The rest of the event is forced into two jets using the DURHAM algorithm. The slim jets are constrained to be in the $20° \leq \theta_\tau \leq 160°$ polar angle region to reduce the Ze^+e^- background, while the hadronic dijet invariant mass is required to be between 20 and 110 GeV/c^2 in order to reduce the $q\bar{q}(\gamma)$ and $Z\gamma^*$ backgrounds. The jet energies and masses are then rescaled, imposing energy and momentum conservation, in order to improve the estimation of the masses of the dijets ($\tau^+\tau^-$ and $q\bar{q}$). Both dijets are required to have a rescaled mass above 20 GeV/c^2 and below $\sqrt{s}$, and each hadronic jet must have a rescaling factor in the range 0.4 to 1.5.

The remaining background comes from genuine $\ell^+\ell^- q\bar{q}$ events. In order to reject the $q\bar{q}$ e^+e^- and $q\bar{q}$ $\mu^+\mu^-$ backgrounds the measured mass of the leptonic dijet is required to be between 10 and 80 GeV/c^2 and its electromagnetic energy to be below 60 GeV (see Figure 5c). The effect of the selections on data, simulated background and signal events is given in Table 1, while the selection efficiencies are summarised in Tables 2 (SM) and 3 (hA). Systematic uncertainties have been estimated by moving each selection cut according to the resolution of the corresponding variable. The main contributions are due to the $\tau^+\tau^-$invariant mass and electromagnetic energy. The total systematic uncertainties amount to $\pm 6\%$ on signal efficiencies and $\pm 11\%$ on the background.

At the end of the above selections, the reconstructed Higgs boson mass is estimated from the sum of the rescaled dijet masses in the hA channel and by subtracting the nominal Z mass in the hZ channels (Figure 5e). Besides this reconstructed mass, the two-dimensional calculation of the confidence levels makes use of a discriminating variable, again using a likelihood technique. This variable is built from the distributions of the rescaling factors of the τ jets, the τ momenta and the global b-tagging x_b variable (see Figure 5g). Since the three possible $\tau^+\tau^- q\bar{q}$ signals are analysed in the same way, the confidence level computation uses only one global $\tau^+\tau^- q\bar{q}$ channel. At each test point, the signal expectation and distribution in this channel are obtained by summing the contributions from the three signals weighted by their expected rates.

6 Higgs boson searches in events with jets and missing energy

The analysis starts with a preselection which is done in two steps. The first step aims at reducing the $\gamma\gamma$ contamination and requires a total charged multiplicity greater than 10 (with at least one charged particle with a transverse momentum above 2 GeV/c), a total charged energy greater than 30 GeV and the sum of the transverse energies of the charged particles with respect to the beam axis greater than 28 GeV. The total transverse momentum has to be greater than 2 GeV/c. Furthermore, events where both the total transverse momentum and the largest single charged particle transverse momentum are less than 5 GeV/c have also been rejected. After these cuts, the $\gamma\gamma$ contamination is reduced to 1.5% of the total background, which is now dominated by $q\overline{q}(\gamma)$ events.

Then, jets are reconstructed from the event particles using the LUCLUS [19] algorithm with the DURHAM distance ($y_{cut} = 0.005$). The results will be hereafter referred to as "free-jet clustering". Events are also forced in a two-jet topology using the same algorithm (with a result referred to as "two-jet clustering") in order to tag specifically $q\overline{q}(\gamma)$ events with the photon emitted along the beam axis. The rest of the preselection is designed to remove a large fraction of the remaining background without affecting the signal efficiency using the good discrimination between background and signal in the distributions of many analysis variables. The selection requires the most energetic electromagnetic cluster associated to a charged particle to be lower than 25 GeV (or 10 GeV if the charged particle associated to the cluster failed the charged particle selection criteria), the effective centre-of-mass energy, $\sqrt{s'}$, to be greater than 100 GeV, the absolute value of the cosine of the polar angle of the missing momentum to be lower than 0.98, the most forward jet in the free-jet clustering to be more than 16° from the beam axis, the fraction of electromagnetic energy per jet in the free-jet clustering to be lower than 0.8, the energy deposited in the forward region within 30° around the beam axis to be smaller than 20 GeV and the energy of the more (less) energetic jet in the two-jet clustering to be between 30 and 90 GeV (10 and 60 GeV). This defines the preselection.

The final discrimination between signal and background is achieved through a multi-dimensional variable built using the likelihood ratio method. The input variables are the effective centre-of-mass energy $\sqrt{s'}$, the global b-tagging variable $x_{\rm b}$, the missing momentum P_{mis}, and the cosine of its polar angle, the charged multiplicities of the jets in the free-jet clustering, the energy of the most energetic jet in the two-jet clustering, E_{jet1}, the acoplanarity, defined as the supplement of the angle between the transverse momenta of the two jets in the two-jet clustering, the maximal (over all particles in an event) transverse momentum with respect to the axis of the closest jet in the two-jet clustering, P_{tmax}, and the output of a veto algorithm based on the response of the lead-scintillator counters installed at polar angles around 40° to detect photons crossing this insensitive region of the electromagnetic calorimeters.

The distributions at preselection level of some of the input variables are shown in Figure 6 while that of the discriminant variable is given in Figure 7. Figure 8 shows the expected background rate as a function of the efficiency for a Higgs mass $m_{\rm h}$=95 GeV/c^2 when varying the cut on the discriminant variable. The final selection yields a total background of $27.8 \pm 1.0(stat.)$ at 54.3% efficiency for the signal. The number of observed events is 27. Table 1 details the effects of the selections on data and simulated samples of background and signal events while the selection efficiencies as a function of the Higgs boson mass are summarised in Table 2.

The systematic uncertainty is dominated by the imperfect modelling of the energy flow. The corresponding error has been estimated by comparing data and simulation in test samples of $Z\gamma$ events at high energy and data taken at the peak. It amounts to 11.0% relative to the background. Other sources include the imperfect modelling of b-tagging and jet angular resolutions, the dependence on the jet algorithm and uncertainties in cross-sections. This yields a total systematic error of $\pm 12.4\%$.

7 Higgs boson searches in pure hadronic events

The aim of the four-jet preselection is to eliminate radiative and $\gamma\gamma$ events and to reduce the QCD and $Z\gamma^*$ background. This preselection, common to HZ and hA analyses, has not changed with respect to last year's analysis [1], except that the number of charged particles for the di-jet recognised as the Z is required to be greater than or equal to five, in order to remove events in which the Z decays into charged leptons.

7.1 The HZ four-jet channel

The present analysis is an update of the method used by DELPHI at 183 GeV [1]. Events are selected using a discriminant variable which is defined as the ratio of likelihood products for signal and background hypotheses for a set of quantities having a different behaviour in the two cases. These variables can be divided into two categories related respectively to the shape and to the b-content of the events. The six shape variables are those defined previously [1] and a new quantity: the fitted mass of the di-jet assigned to the Z. The agreement between data and background simulation is illustrated at preselection level in Figure 9 which shows the distributions of four analysis variables.

In the previous version of this analysis the Z boson mass was fixed at its nominal value and the "best" pairing of jets to select the Higgs and Z candidates was found by maximising an expression in which the b-content of the different jets and the χ^2 probability of the five-constraint fit contribute. When the production of the Higgs boson is close to the kinematic limit, the Z mass distribution no longer has a Breit-Wigner shape centred on m_Z . The previous procedure has been generalised using the Z mass distribution given by the simulation for a fixed Higgs mass equal to 95 GeV/c^2. For values of the Higgs mass which differ from 95 GeV/c^2, the same Z mass distribution has been used, even if not optimal, in order to be independent of the assumed value for the Higgs mass. The resulting mass distribution, for preselected events in data and simulation, is shown in Figure 10.

Events originating from the signal and from the background are separated using the value of a discriminant variable. This variable combines the information from shape variables to reduce the QCD background and from the b-tagging variable to reduce the contribution of W pairs. The most effective variable against the W^+W^- background was found to be x_b^i, the combined b-tagging variable [12] measured for each jet. The likelihoods that each event is of HZ, W^+W^- or QCD origin are evaluated. The final discriminant variable is obtained as the ratio between signal and background likelihoods. Figure 11 shows the number of expected Monte-Carlo and observed data events, as a function of the efficiency on the signal when cutting on this discriminant variable.

The two-dimensional distribution obtained by combining the Higgs mass estimate and the likelihood ratio is used for the final limit calculation. The most background-like events are suppressed by demanding that the (log)likelihood ratio be greater than -1.0.

The systematic uncertainties have been evaluated by considering a b-tagging, a QCD related and a 4-fermion part, independently, together with an uncertainty on the cross-sections of all processes, resulting in an overall relative uncertainty of 7.5% at the final selection level.

7.2 The hA four–b channel

A likelihood method has been applied to search for hA production in the four–jet channel. After the common four–jet preselection, tighter cuts were applied to the remaining events, namely, a cut in the parameter of the DURHAM algorithm ($y_{cut} \geq 0.003$) is imposed as well as the requirement of at least two charged particles per jet. Finally, an event is rejected if its maximum inter-jet energy difference is greater than 70 GeV. The resulting number of expected events and the signal efficiencies after this preselection are given in Table 1.

The following eight variables are combined in the likelihood: the event thrust, the second and fourth Fox-Wolfram moments, H_2 and H_4, the minimal (among the three possible pairings of jets) di-jet-masses difference, the production angle of the candidate bosons, the sum (over the four jets) of the b–tag jet variable, the minimum di-jet b–tag and the number of secondary vertices. For each event, the measured value of each of these discriminant variables is compared with probability density functions obtained from simulated events.

Figure 12 shows the resulting efficiency versus the total background varying the likelihood cut (assuming $m_{\mathrm{A}} = 80$ GeV/c^2 and $\tan\beta = 20$). The final cut value is chosen depending on the efficiency–background point desired; for the derivation of the limits, a cut on the likelihood output at 2.0 has been chosen. A total of 13 events is observed while 11.41 are expected. A more stringent cut on the likelihood output corresponding to a requirement at 3.05 is used for the mass plot (see Fig 13). This yields a total background of 4.72 ± 0.22 coming from $\mathrm{q\bar{q}}(\gamma)$(2.11 ± 0.14) and 4-fermion processes (2.61 ± 0.17) and 3 events selected in data with a sum of their di-jet masses of 147, 180 and 176 GeV/c^2. Efficiencies obtained for different masses and $\tan\beta$ are summarised in Table 3.

To check systematic uncertainties on the total background due to the modeling of the shape of the probability density functions, the training and validation sample were exchanged and the analysis repeated. The uncertainty on the total background due to this effect has been estimated at the level of 5% and has been added (quadratically) to the other sources of errors, in particular the one coming from the b-tagging estimation, resulting in a final relative systematic uncertainty of 8%.

8 Summary and results

The results of the searches presented in the previous sections can be translated into exclusion limits on the masses of the neutral Higgs bosons in the SM and MSSM.

8.1 Summary

For each analysis of the HZ and hA channels at 188.7 GeV, the integrated luminosity, the expected backgrounds and their errors, and the number of observed events at various levels of the analyses are summarised in Table 1. Within each channel, the penultimate line represents the inputs for the confidence level calculations ("final selection"), while

Selection	Data	Total background	$q\bar{q}(\gamma)$	4 fermion	Efficiency
Electron channel 155.4 pb^{-1}					
Preselection	1290	1227.4	924	267	78.5
tight lepton id.	28	27.9± 0.9	13	12.4	61.0
final selection	5	6.63±0.26	1.29	5.34	58.1
$x_b > -1.8$	1	2.50±0.17	0.58	1.92	49.6
Muon channel 158.0 pb^{-1}					
Preselection	6441	6177	4871	1239	84.8
tight lepton id.	15	15.5 ± 0.7	1.96	13.6	75.0
final selection	5	5.09 ± 0.19	0.09	5.00	70.8
$x_b > -1.74$	2	1.69±0.12	0.02	1.67	60.5
Tau channel 158.0 pb^{-1}					
Preselection	7128	7091	4810	2281	95.8
$\ell^+\ell^- q\bar{q}$	21	20.4± 0.5	3.8	16.6	31.4
final selection	11	11.54±0.39	1.73	9.81	29.9
$\mathcal{L} > 0.83$	0	0.77±0.03	0.03	0.74	18.1
Missing energy channel 153.3 pb^{-1}					
Anti $\gamma\gamma$	14294	13623.2	10854.6	2563.2	84.3
Preselection	1183	1152.9	705.9	430.9	77.3
$\mathcal{L} > 2.55$	27	27.8± 1.0	17.1	10.1	54.3
$\mathcal{L} > 4.4$	4	6.0±0.22	3.1	2.9	33.9
Four-jet channel 158.0 pb^{-1}					
Preselection	1730	1706.2	583	1123	87.1
$\mathcal{L} > -1.0$	136	122.9± 1.1	26.8	96.1	63.3
$\mathcal{L} > 0.28$	24	24.9± 0.2	7.2	17.7	45.9
hA four-jet channel 158.0 pb^{-1}					
Preselection	1327	1274	318	956	85.9
$\mathcal{L} > 2.0$	13	11.41± 0.34	5.19	6.22	65.5
$\mathcal{L} > 3.05$	3	4.72± 0.15	2.11	2.61	55.0

Table 1: *Effect of the selection cuts on data, simulated background and simulated signal events at* $\sqrt{s}$ *= 188.7* GeV. *Efficiencies (in %) are given for the signal, ie.* m_H *= 95* GeV/c^2 *for the SM and* m_A *= 80* GeV/c^2, $\tan\beta$ *= 20 for the MSSM. Within each channel, the last line gives the entries for the mass-plot, while the preceding line represent the inputs for the limit derivation. The quoted errors are statistical only.*

m_{H} (GeV/c^2)	Electron channel	Muon channel	$\mathrm{H}\tau^+\tau^-$ channel	$\tau^+\tau^-\mathrm{Z}$ channel	Mis. Energy channel	Four-jet channel
70.0	$55.4^{+1.9}_{-2.7}$	$68.3^{+1.5}_{-1.6}$	28.1 ± 3.0	32.0 ± 3.5	20.6 ± 2.0	52.2 ± 4.1
75.0	$56.8^{+1.4}_{-2.2}$	$71.2^{+1.3}_{-1.4}$	28.3 ± 3.0	30.8 ± 3.3	32.3 ± 3.0	54.6 ± 4.2
80.0	$58.1^{+1.3}_{-2.5}$	$73.4^{+1.2}_{-1.0}$	28.1 ± 3.0	31.5 ± 3.5	43.5 ± 4.0	58.7 ± 4.5
85.0	$57.8^{+1.1}_{-2.0}$	$72.2^{+1.4}_{-1.4}$	27.6 ± 3.1	29.9 ± 3.2	52.0 ± 4.6	58.8 ± 4.5
90.0	$59.0^{+1.1}_{-2.4}$	$73.7^{+1.3}_{-1.4}$	26.6 ± 2.8	30.6 ± 3.2	57.1 ± 5.1	62.4 ± 4.7
95.0	$58.1^{+1.2}_{-2.2}$	$70.8^{+1.2}_{-1.1}$	25.9 ± 2.7	29.9 ± 3.1	54.3 ± 4.8	63.3 ± 4.7
100.0	$55.5^{+1.2}_{-3.8}$	$62.0^{+1.7}_{-1.6}$	26.3 ± 2.8	28.2 ± 3.0	45.5 ± 4.1	56.7 ± 4.3

Table 2: hZ channels: *efficiencies (in %) of the selection at* $\sqrt{s} = 188.7\,\mathrm{GeV}$ *as a function of the mass of the Higgs boson. The quoted errors include systematic uncertainties.*

$\tan\beta = 20$			$\tan\beta = 2$		
m_{A} (GeV/c^2)	Four-jet channel	Tau channel	m_{A} (GeV/c^2)	Four-jet channel	Tau channel
70.0	58.6 ± 5.0	32.4 ± 3.4	70.0	51.8 ± 4.4	13.5 ± 1.5
75.0	60.5 ± 5.0	33.1 ± 3.4	75.0	54.7 ± 4.5	16.7 ± 1.8
80.0	65.5 ± 5.3	32.2 ± 3.3	80.0	58.4 ± 4.8	25.8 ± 2.7
85.0	64.7 ± 5.3	31.8 ± 3.4	85.0	60.0 ± 4.9	33.7 ± 3.6
90.0	60.6 ± 5.0		90.0	61.1 ± 5.1	

Table 3: hA channels: *efficiencies (in %) of the selection at* $\sqrt{s} = 188.7\,\mathrm{GeV}$ *as a function of the mass of the A boson for two values of* $\tan\beta$*(20 and 2). The quoted errors include systematic uncertainties.*

the last line gives the result of a tighter selection. The efficiencies versus Higgs mass at the final selection level can be seen in Table 2 (SM channels) and Table 3 (MSSM channels). The errors are obtained by summing the statistical and systematic uncertainties quadratically.

8.2 The SM Higgs boson

As an illustration, Figure 14 shows the distribution of the reconstructed Higgs boson mass found in the HZ channel after the tight selection (last lines in Table 1) for data, simulated background and signal events. The last cut in each channel has been chosen such that the signal-over-background ratio (for the reference mass) be almost equal for all channels (between .2 and .35). Within the 188.7 GeV data, the total number of events observed in all channels is 31, which is consistent with the 35.9 expected background. Since the two hypotheses (background only and background plus signal at 95 GeV/c^2) are almost indistinguishable, a possible signal at 90 GeV/c^2 has been superimposed in order to visualise our resolution in the mass of such a signal.

We proceed to set a limit on the SM Higgs boson mass, combining these data with those taken at lower energies, namely 161,172 GeV [14] and 183 GeV [1]. The expected cross-sections and branching ratios are taken from [20,21], with the top mass set to 175 GeV/c^2.

The confidence levels CL_b, CL_{sb} and CL_s are computed as described in [1]. CL_b and CL_{sb} are the confidence levels in these hypotheses (background only and signal + background), while CL_s is conservatively taken as their ratio (CL_{sb}/CL_b).

In the presence of a sizeable Higgs signal the value of the observed CL_b (top of Figure 15) would approach one, because it measures the fraction of background-only experiments which are less signal-like than the observation. On the contrary here, the observation agrees well with the expectation (background only). Furthermore the curve for the signal hypothesis shows that the expected 5σ discovery limit (horizontal line at $1 - CL_b = 5.7 \times 10^{-7}$) is at 88.6 GeV/$c^2$. The confidence level in the signal is shown in Fig. 15 (bottom). The observed 95% CL lower limit on the mass is $m_{\mathrm{H}} > 94.6$ GeV/c^2, while the expected mean is 94.4 GeV/c^2 and the expected median (50% exclusion potential) is 95.3 GeV/c^2. If errors had not been allowed for, the observed (expected) limit would have been increased by 0.2 GeV/c^2 (0.4 GeV/c^2).

The effective $\Delta\chi^2$ ($-2\Delta \ln \mathcal{L}$) with which the SM Higgs is excluded is shown in Fig. 16. In the event of a discovery the $\Delta\chi^2$ would be negative, and could be used to extract the mass and its error, as can be seen on the bottom plot of Fig. 16.

Finally the data can be used to set 95% CL upper bounds on the HZZ coupling in non-standard models which assume that the Higgs boson decay properties are identical to those in the SM but the cross-section may be different. Figure 17 shows the excluded cross-section as a function of the test mass.

8.3 Neutral Higgs bosons in the MSSM

The results in the hZ and hA processes are combined with the same statistical method as for the SM, using also earlier results at LEP2 energies [1,14,22].

In the MSSM, at tree level, the production cross-sections and the Higgs branching fractions depend on two free parameters, $\tan\beta$ and one Higgs boson mass, or, alternatively, two Higgs boson masses, eg m_{A} and m_{h}. The properties of the MSSM Higgs bosons are modified by radiative corrections which introduce additional parameters: the

mass of the top quark, the Higgs mixing parameter, μ, the common sfermion mass term at the EW scale, M_S, the common SU(2) gaugino mass term [1] at the EW scale, M_2, and the common squark trilinear coupling at the EW scale, A. The interpretation of the experimental results depends on the values assumed for these parameters as well as on the order of the calculated radiative corrections.

The results described hereafter rely on leading-order two-loop calculations of the radiative corrections in the renormalization group approach [23], with recent modifications (about top threshold and gluino two-loop corrections) that make the computations agree with fully diagrammatic two-loop calculations [24]. After these improvements, the benchmark prescriptions for the parameters beyond tree-level have also been refined, leading to two extreme scenarii for the theoretical upper bound on $m_{\rm h}$ as a function of $\tan\beta$ [25] which differ only by the value of $X_t = A - \mu\cot\beta$, the parameter which controls the mixing in the stop sector. In the following, we adopt these new prescriptions which correspond to: 175 GeV/c^2 for the top mass, 1 TeV/c^2 for M_S, 200 GeV/c^2 for M_2 and -200 GeV/c^2 for μ. Two values have been considered for the mixing in the stop sector: $X_t = \sqrt{6}M_S$, which defines the so-called $m_{\rm h}^{max}$ scenario, and $X_t = 0$, which defines the no mixing scenario. Then a scan is made over the MSSM parameters $\tan\beta$ and $m_{\rm A}$, in the $m_{\rm A}$ range [2] of 20 GeV/c^2 - 1 TeV/c^2, and $\tan\beta$ between 0.5 and 50. At each point of the parameter space, the hZ and hA cross-sections and the Higgs branching fractions are computed with the `HZHA03` [10] program.

The signal expectations in each channel are derived from the cross-sections, the experimental luminosity and the efficiencies. A correction is applied to account for differing branching fractions of the Higgs bosons into $b\bar{b}$ and $\tau^+\tau^-$ between the input point and the simulation (e.g. for the hZ process, the simulation is done in the SM framework). For the hA channels, as there can be a difference between the masses of the h and A bosons at low $\tan\beta$, the set of hA efficiencies obtained from the simulation at $\tan\beta = 20$ is applied at all points with $\tan\beta$ above 2.5, while the set of efficiencies derived from the $\tan\beta = 2$ simulation is applied below. The same holds for the discriminant information. The signal expectations, expected backgrounds and numbers of candidates enter in the computation of the observed confidence level in the signal hypothesis at the input point, CL_s. The expected confidence level in the signal hypothesis is also derived at each point. As there is a large overlap in the background selected by the two four-jet channels, only one channel is selected at each input point, on the basis of the best signal over background ratio. This ensures that the channels which are combined in the confidence level computations are independent.

The results translate into regions of the MSSM parameter space excluded at 95% CL or more. The excluded regions are presented in the ($m_{\rm h}$, $\tan\beta$) plane in Fig. 18, in the ($m_{\rm A}$, $\tan\beta$) plane in Fig. 19 and in the ($m_{\rm A}$, $m_{\rm h}$) plane in Fig. 20. As illustrated in the latter, there is a small region of the parameter space where the decay h$\rightarrow$AA opens, in which case it supplants the h$\rightarrow b\bar{b}$ decay. But, due to the high luminosity collected at 188.7 GeV, the results in the h$\rightarrow b\bar{b}$ channel alone cover most of the area which remained unexcluded at 183 GeV in this region [1].

Finally, the results shown in Figs. 18, 19 and 20 establish 95% CL lower limits on $m_{\rm h}$ and $m_{\rm A}$, whatever the assumption on the mixing in the stop sector and for all values of $\tan\beta$ greater than or equal to 0.6:

$$m_{\rm h} > 82.6 \text{ GeV}/c^2 \qquad m_{\rm A} > 84.1 \text{ GeV}/c^2.$$

[1] The U(1) and SU(3) gaugino mass terms at the EW scale, M_1 and M_3, are assumed to be related to M_2 through the GUT relations $M_1 = (5/3)\tan^2\theta_{\rm w} M_2$ and $M_3 = (\alpha_s/\alpha)\sin^2\theta_{\rm w} M_2$.

[2] The region $m_{\rm A}$ below 20 GeV/c^2 would need LEP1 results which are not yet available in the format required by the statistical procedure.

The expected limits are 81.3 GeV/c^2 in $m_{\rm h}$ and 82.3 GeV/c^2 in $m_{\rm A}$. In the low $\tan\beta$ region, in the no mixing case, all values of $m_{\rm A}$ up to 1 TeV/c^2 are excluded, providing an excluded range in $\tan\beta$ between 0.6 and 2.2, in agreement with the expected excluded range. On the other hand, no limit can be set on $\tan\beta$ in the $m_{\rm h}^{max}$ scenario (see Fig. 19).

8.4 Interpretation in a general Two Higgs Doublet Model

These results can also be translated to the framework of a general Two Higgs Doublet Model (2HDM) with one assumption (the decay of both h and A is dominated by $\rm b\bar{b}$ and/or $\rm c\bar{c}$ final states) and two options: CP conserving or CP violating.

In the CP–conserving two Higgs doublet model, the h and H bosons are mixtures of the real parts of the neutral Higgs fields, while A derives from the imaginary components not absorbed by the Z. The coupling strengths are: $C_{\rm hZ} = \sin(\alpha-\beta)$ and $C_{\rm hA} = \cos(\alpha-\beta)$. These couplings clearly indicate the complementarity of the two processes. Besides, if one of them is experimentally out of reach for a given set of masses, no exclusion is possible since mixing angles could always be such that the other process is suppressed below detectability.

The exclusion plot (left of Figure 21) is obtained in the following way: for each pair of $m_{\rm h}$ and $m_{\rm A}$ values the number of expected events for the channels hA and hZ is calculated using the cross-sections, integrated luminosities, branching ratios and efficiencies quoted in this paper. This number depends obviously on the factors $C_{\rm hZ}$ and $C_{\rm hA}$. Thus a minimisation of the confidence level with respect to these factors has been performed, taking into account the sum rule $C^2_{\rm hZ} + C^2_{\rm hA} = 1$.

It should be noted that in 2HDM the branching ratios of A and h into $\rm b\bar{b}$ are proportional to $\tan\beta$ and $\sin\alpha/\cos\beta$ respectively. Imposing the condition $|\sin\alpha| > \cos\beta$, which is barely restrictive for medium or large values of $\tan\beta$, leads to a dominant coupling to b quarks for both h and A bosons, (Zone I in Figure 21)

The case of non–b decays has also been studied, using the selections of this paper except those referring to b–tagging. This takes care of a scenario with $\tan\beta < 1$ which would allow a dominant decay of the Higgs boson into $\rm c\bar{c}$ [26]. This region (named Zone II in Figure 21) occurs for values of the α and β angles such that $\alpha \sim \beta \sim 0$, resulting in a very restrictive and particular parameter set of the 2HDM which represents the most pessimistic scenario in this kind of search. Any other situation will lead to an intermediate excluded region, as for example when $\sin\alpha = 0$ but $\tan\beta > 1$ which implies $\rm q\bar{q}$ $\rm b\bar{b}$ decays of the hA signal.

CP violation in the SUSY sector is an open possibility and may even be necessary in the electroweak baryogenesis scenario (see for instance [27] and references therein). The violation leads to three neutral Higgs bosons with undefined CP properties. It is shown in [28] that the previous sum rule, valid in the CP–conserving case, can be extended to the CP–violating model, giving the relation: $C^2_{\rm hZ} + C^2_{\rm AZ} + C^2_{\rm hA} = 1$, which together with the results described in this paper allows the minimum number of events for each point ($m_{\rm h}$,$m_{\rm A}$) to be calculated, with an extended procedure similar to the one used previously, leading to the excluded region at 95% CL shown in the right plot of Figure 21 (only the conditions for Zone I were used in this case).

Note the perfect symmetry of the figure due to the new AZ channel and thus the opening of the $\rm A \to hh$ decay mode.

This analysis shows that it is possible to exclude a large region of Higgs boson masses even when relaxing the standard assumptions made in the MSSM scenario.

9 Conclusions

The 158 pb^{-1} of data taken by DELPHI at 188.7 GeV, combined with our lower energy data, sets the lower limit at 95% CL on the mass of the Standard Model Higgs boson at:

$$m_{\mathrm{H}} > 94.6 \text{ GeV}/c^2.$$

The MSSM studies described above give for all values of $\tan\beta$ above 0.6, and assuming $m_{\mathrm{A}} > 20$ GeV/c^2:

$$m_{\mathrm{h}} > 82.6 \text{ GeV}/c^2 \qquad m_{\mathrm{A}} > 84.1 \text{ GeV}/c^2.$$

Other LEP experiments, using their data sets collected concurrently with the ones used in this work, have reported similar results [29,30].

Acknowledgements

We are greatly indebted to our technical collaborators, to the members of the CERN-SL Division for the excellent performance of the LEP collider, and to the funding agencies for their support in building and operating the DELPHI detector.
We acknowledge in particular the support of
Austrian Federal Ministry of Science and Traffics, GZ 616.364/2-III/2a/98,
FNRS–FWO, Belgium,
FINEP, CNPq, CAPES, FUJB and FAPERJ, Brazil,
Czech Ministry of Industry and Trade, GA CR 202/96/0450 and GA AVCR A1010521,
Danish Natural Research Council,
Commission of the European Communities (DG XII),
Direction des Sciences de la Matière, CEA, France,
Bundesministerium für Bildung, Wissenschaft, Forschung und Technologie, Germany,
General Secretariat for Research and Technology, Greece,
National Science Foundation (NWO) and Foundation for Research on Matter (FOM), The Netherlands,
Norwegian Research Council,
State Committee for Scientific Research, Poland, 2P03B06015, 2P03B1116 and SPUB/P03/178/98,
JNICT–Junta Nacional de Investigação Científica e Tecnológica, Portugal,
Vedecka grantova agentura MS SR, Slovakia, Nr. 95/5195/134,
Ministry of Science and Technology of the Republic of Slovenia,
CICYT, Spain, AEN96–1661 and AEN96-1681,
The Swedish Natural Science Research Council,
Particle Physics and Astronomy Research Council, UK,
Department of Energy, USA, DE–FG02–94ER40817.

References

[1] DELPHI Collaboration, P. Abreu et al., Eur. Phys. J. **C10** (1999) 563.
[2] LEP Higgs working group report, CERN-EP 99-060, April 1999.
[3] DELPHI Collaboration, P. Aarnio et al., Nucl. Instr. Meth. **303** (1991) 233.
[4] T. Sjöstrand, Comp. Phys. Comm. **39** (1986) 347.
[5] S. Jadach, B.F.L. Ward, Z. Was, Comp. Phys. Comm. **79** (1994) 503.
[6] F.A. Berends, R. Pittau and R. Kleiss, Comp. Phys. Comm. **85** (1995) 437.
[7] S. Nova, A. Olchevski and T. Todorov, in CERN Report 96-01, Vol. 2, p. 224 (1996).
[8] F.A. Berends, P.H. Daverveldt and R. Kleiss, Nucl. Phys. **B253** (1985) 421; Comp. Phys. Comm. **40** (1986) 271, 285 and 309.
[9] F.A. Berends, R. Kleiss, W. Hollik, Nucl. Phys. **B304** (1988) 712.
[10] P. Janot, in CERN Report 96-01, Vol. 2, p. 309 (1996).
For most recent updates, see also http://alephwww.cern.ch/janot/Generators.html.
[11] DELPHI Collaboration, P. Abreu et al., Nucl. Instr. Meth. **A378** (1996) 57.
[12] G. Borisov, Nucl. Instr. Meth. **A417** (1998) 384.
[13] DELPHI Collaboration, P. Abreu et al., Eur. Phys. J. **C10** (1999) 415.
[14] DELPHI Collaboration, P. Abreu et al., Eur. Phys. J. **C2** (1998) 1.
[15] DELPHI Collaboration, P. Abreu et al., Phys. Lett. **B462** (1999) 410.
[16] DELPHI Collaboration, P. Abreu et al., Eur. Phys. J. **C2** (1998) 581 (Sect. 5.2.)
[17] P. Abreu et al., Nucl. Instr. Meth. **A427** (1999) 487.
[18] A.L. Read, *Optimal statistical analysis of search results based on the likelihood ratio and its application to the search for the MSM Higgs boson at 161 and 172* GeV, DELPHI note 97-158 PHYS 737.
[19] T. Sjöstrand, Comp. Phys. Comm. **28** (1983) 227.
[20] E. Gross, B.A. Kniehl, G. Wolf, Zeit. Phys. **C63** (1994) 417; err. ibid. **C66** (1995) 321.
[21] A. Djouadi, M. Spira and P.M. Zerwas, Zeit. Phys. **C70** (1996) 427.
A. Djouadi, J. Kalinowski and P.M. Zerwas, DESY Report 95-211.
[22] DELPHI Collaboration, P. Abreu et al., Zeit. Phys. **C73** (1996) 1.
[23] M. Carena, M. Quiros and C. Wagner, Nucl. Phys. **B461** (1996) 405.
[24] S. Heinemeyer, W. Hollik and G. Weiglein, DESY 99-120 or hep-ph/9909540.
[25] M. Carena, S. Heinemeyer, C.E.M. Wagner and G. Weiglein, CERN-TH/99-374.
[26] DELPHI Collaboration, P. Abreu et al., Zeit. Phys. **C67** (1995) 69-79.
[27] *Electroweak Baryogenesis and Higgs Physics*, M. Carena and C.E.M. Wagner, hep-ph/9704347, April 1997.
[28] J.F.Gunion et al., Phys. Rev. Lett. **79** (1997) 982.
[29] L3 Collaboration, M.Acciarri et al., Phys. Lett. **B461** (1999) 376. (SM Higgs only)
[30] OPAL Collaboration, CERN-EP/99-096, Subm. to Eur. Phys. J. C.

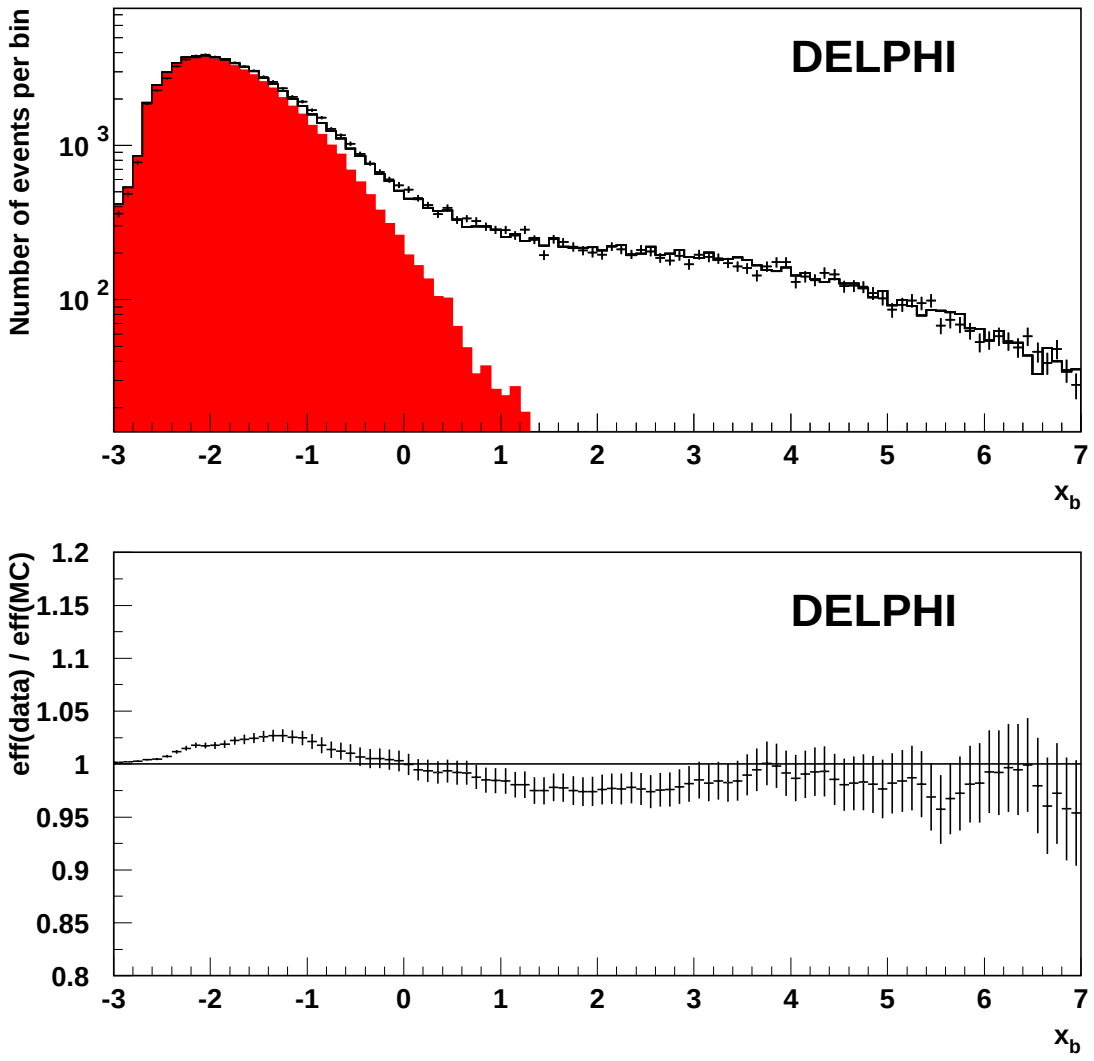

Figure 1: *Distributions of the combined b-tagging variable* x_{b}*, in data (points) and simulation (histogram). The contribution of udsc-quarks is shown as the dark histogram. Bottom: the ratio of the tagging rates in the data and the simulation as a function of the cut in the b-tagging variable.*

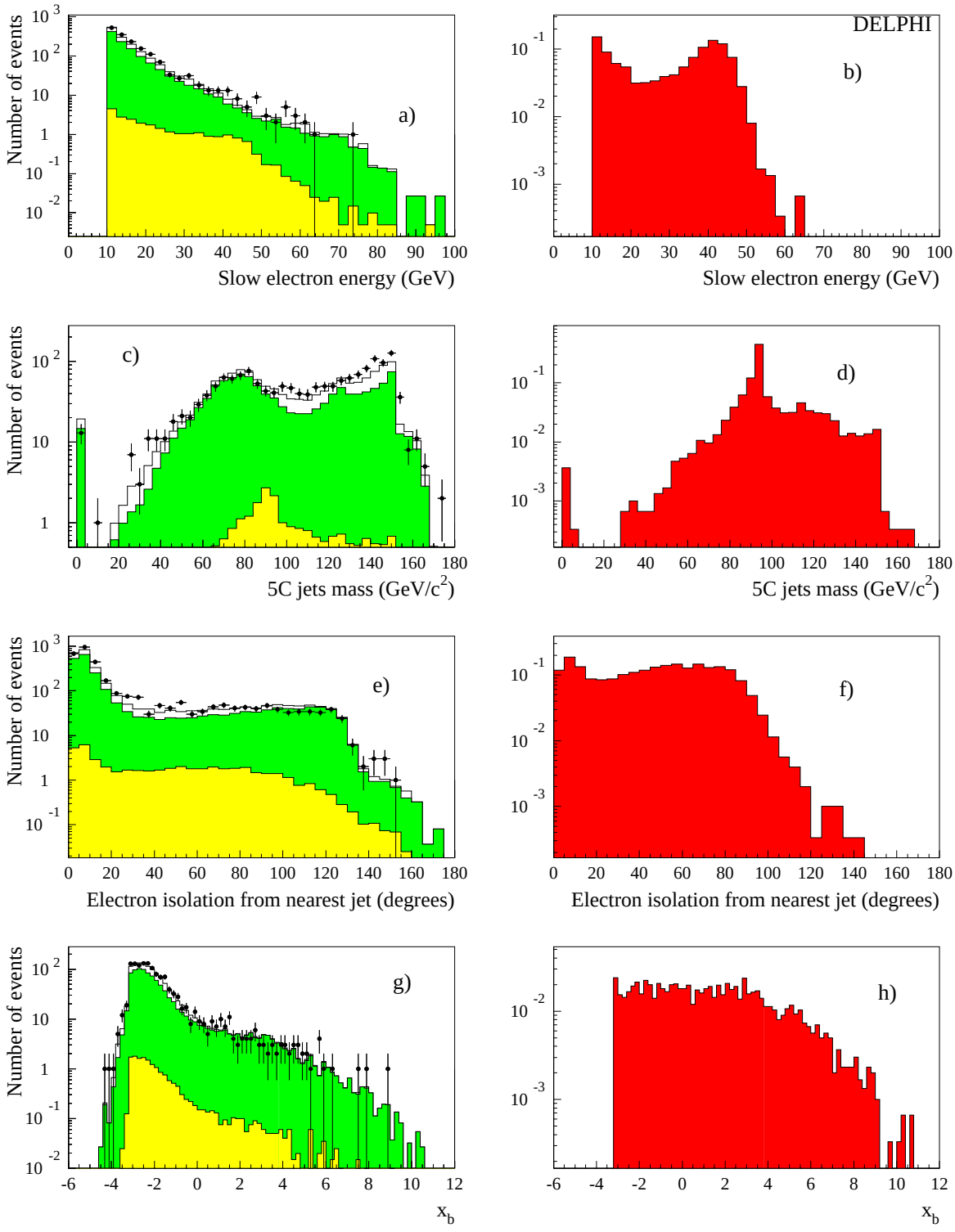

Figure 2: He^+e^-channel: *distributions of some analysis variables as described in the text, at the preselection level. The plots on the left-hand side show a comparison between 188.7* GeV *data (dots) and simulated background events (solid line) normalised to the experimental luminosity. The dark grey areas represent the contribution of the* $q\bar{q}(\gamma)$ *background and the light grey area the* $e^+e^-q\bar{q}$ *contribution. The expected normalised distributions of the same variables for a signal at 95* GeV/c^2 *are represented on the right-hand side. Note the different y-scales.*

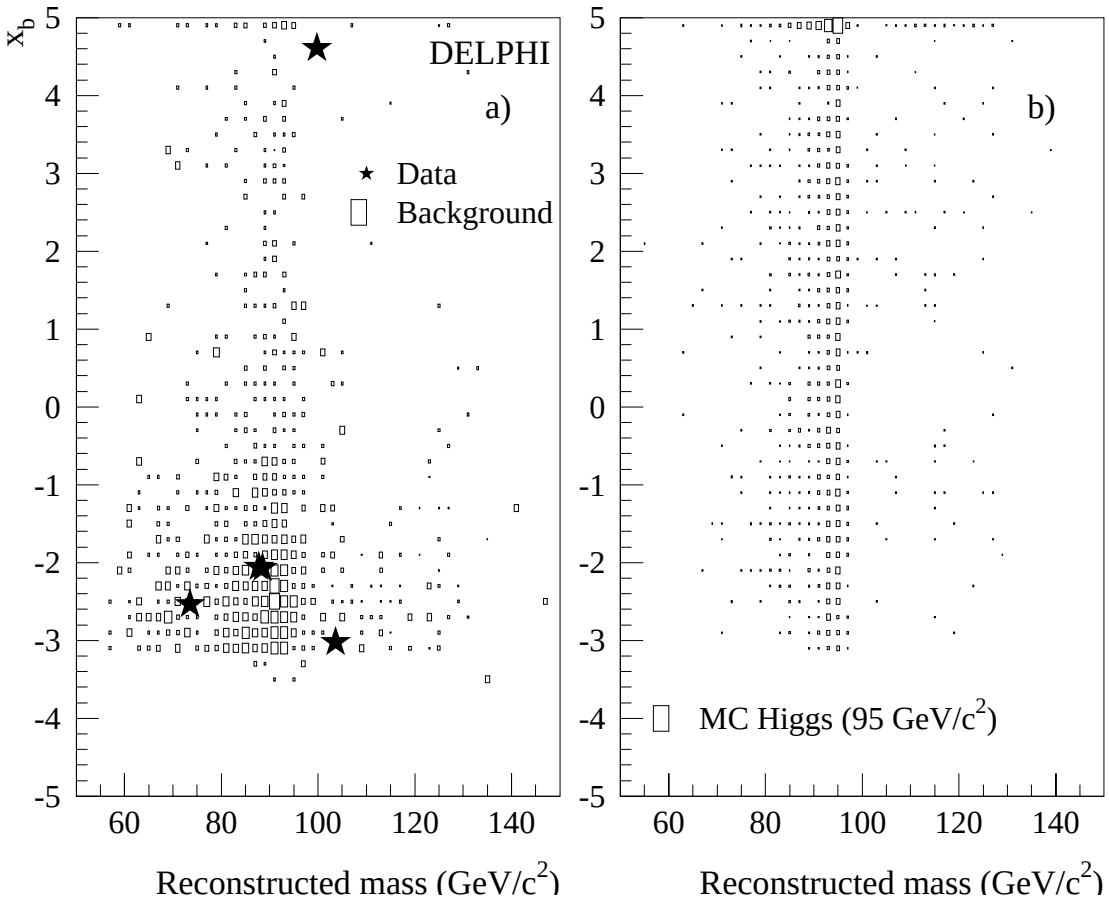

Figure 3: $\mathrm{He^+e^-}$channel: *distributions of the global b-tagging variable versus the fitted recoil mass for data, background and simulated signal events with* $m_{\mathrm{H}} = 95$ GeV/c^2 *at 188.7* GeV. *These distributions are the inputs for the Confidence Levels computation.*

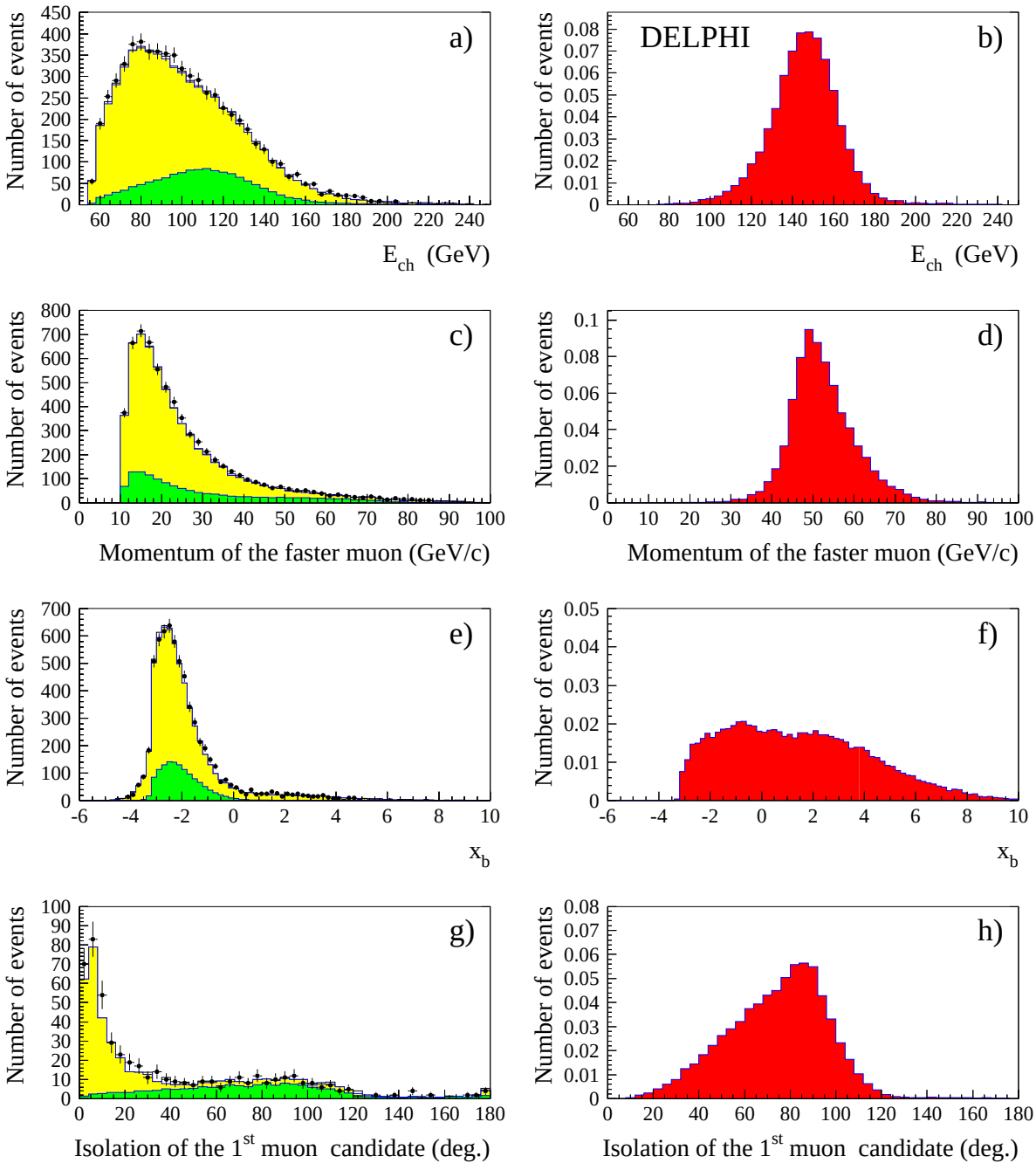

Figure 4: H$\mu^+\mu^-$ channel: *distributions of some analysis variables as described in the text, at the preselection level (a to f) or after the lepton pair selection (g and h). The dark grey area represents the contribution of the* $q\bar{q}(\gamma)$ *background and the light grey area the 4 fermions contribution. The expected normalised distribution for the signal (with* $m_H = 95$ GeV/c^2*) is represented on the right-hand column.*

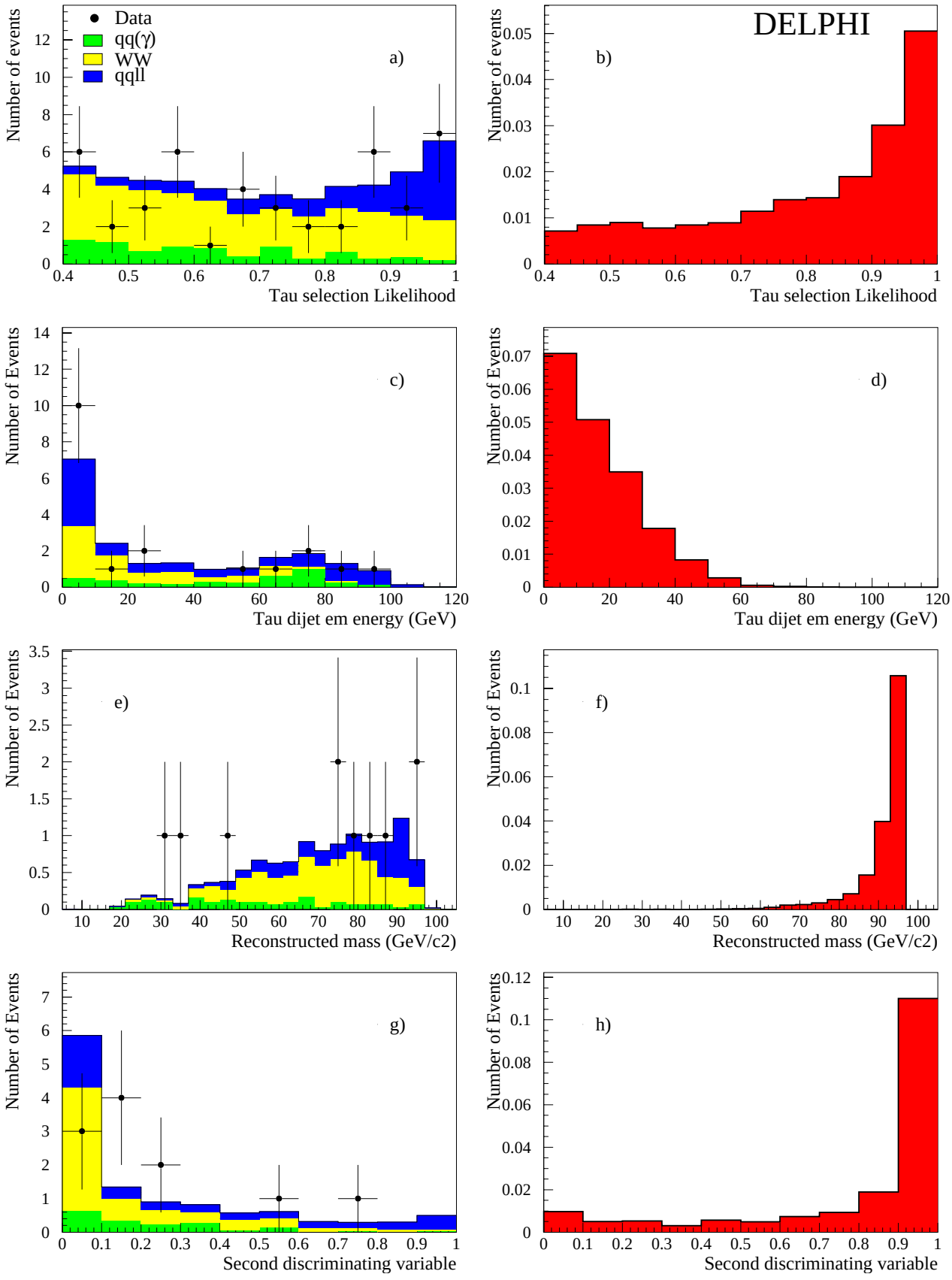

Figure 5: $(\mathrm{H} \to \mathrm{q\bar{q}})\tau^+\tau^-$ channel : *distributions of some variables used in the analysis. a): τ selection likelihood, c): τ dijet electromagnetic energy, e): reconstructed Higgs boson mass, g): global likelihood. The signal (for m_{H} =95 GeV/c^2) on the right-hand side is normalised to the observed luminosity.*

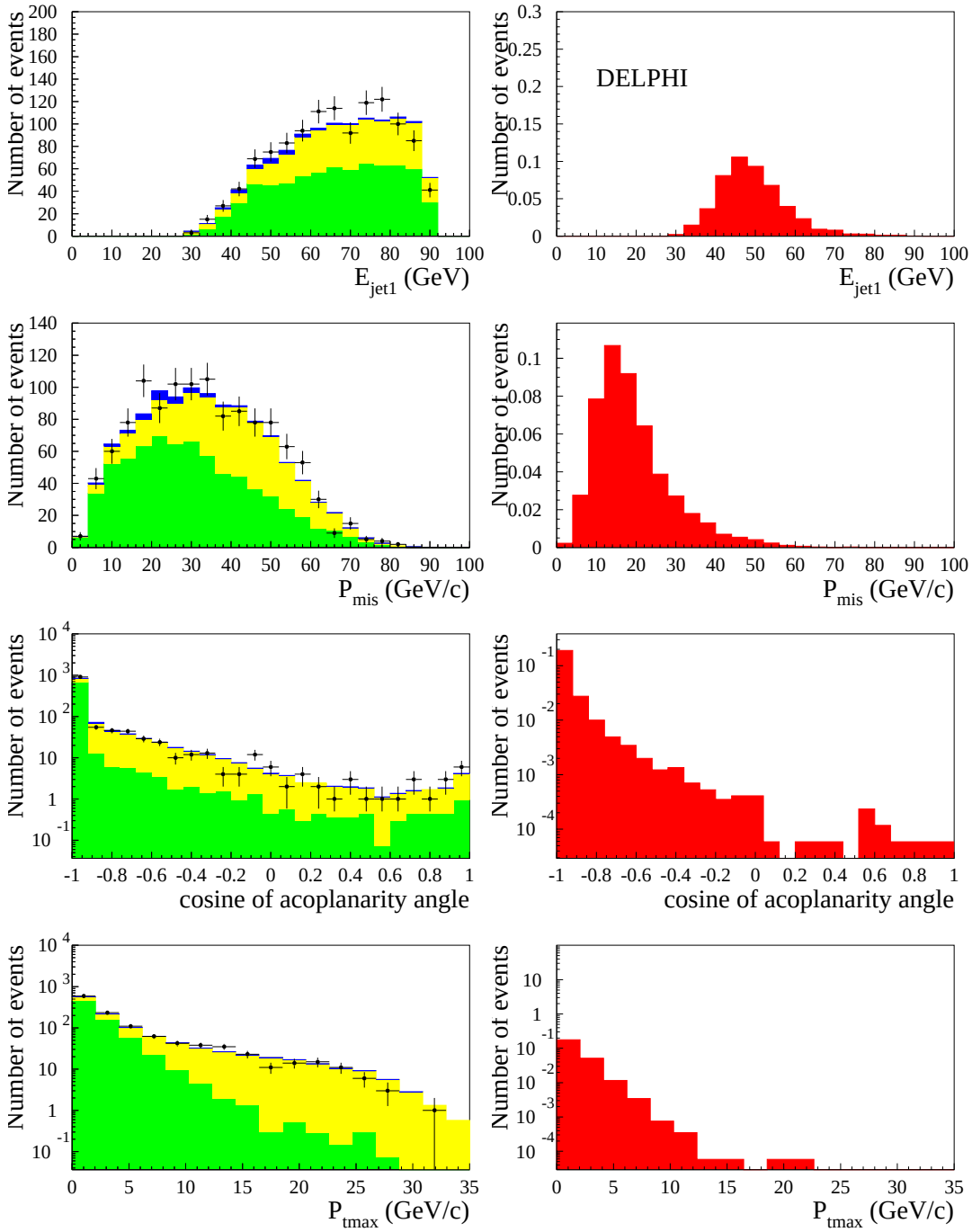

Figure 6: H$\nu\bar{\nu}$ channel: *distributions of the main analysis variables as described in the text, at the preselection level. The points with error bars represent the data. The left hand side histograms show the different backgrounds and the right hand side histograms show the signal distributions for* $m_{\mathrm{H}} = 95$ GeV/c^2.

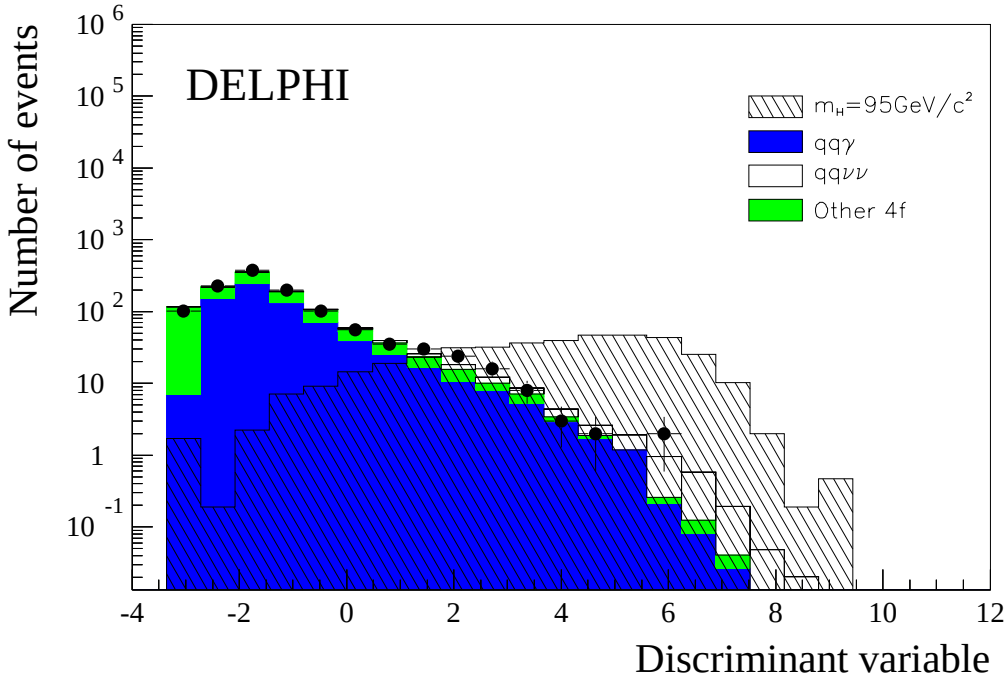

Figure 7: H$\nu\bar{\nu}$ channel: *Distributions of the discriminant variable for the expected background events (full histograms), data (points) and a Higgs signal with* $m_{\mathrm{H}} = 95$ GeV/c^2 *(dashed histogram) are shown. The normalisation for the Higgs signal is 100 times the expectation.*

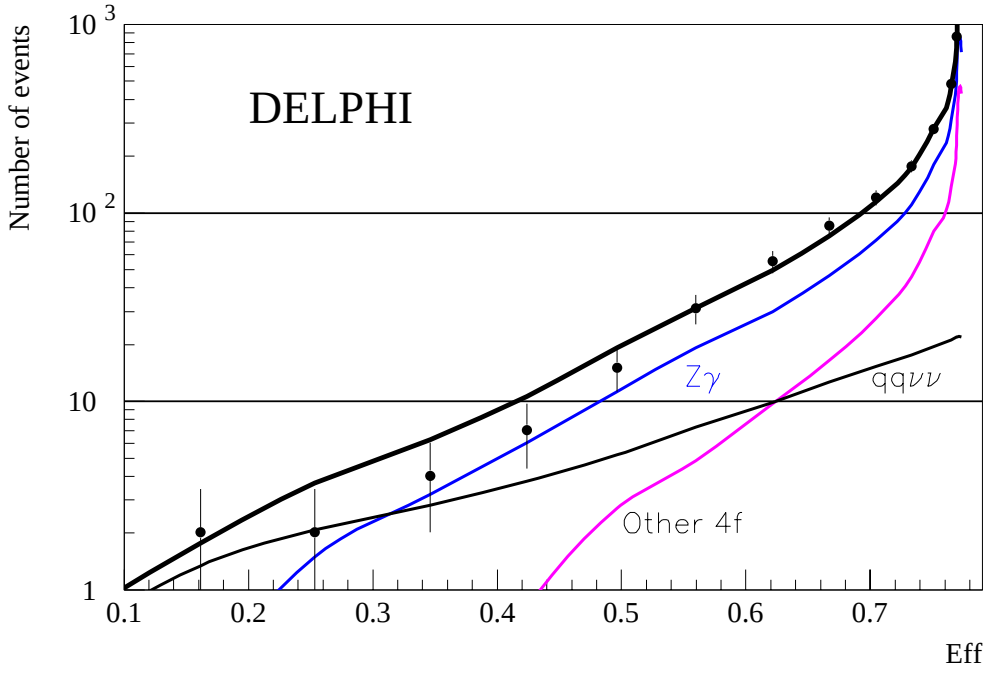

Figure 8: H$\nu\bar{\nu}$ channel: *Efficiency versus total background as a result of varying the cut on the Likelihood. The contribution of different backgrounds are shown separately. Points with error bars are the data, and the thick black line shows the total expected background.*

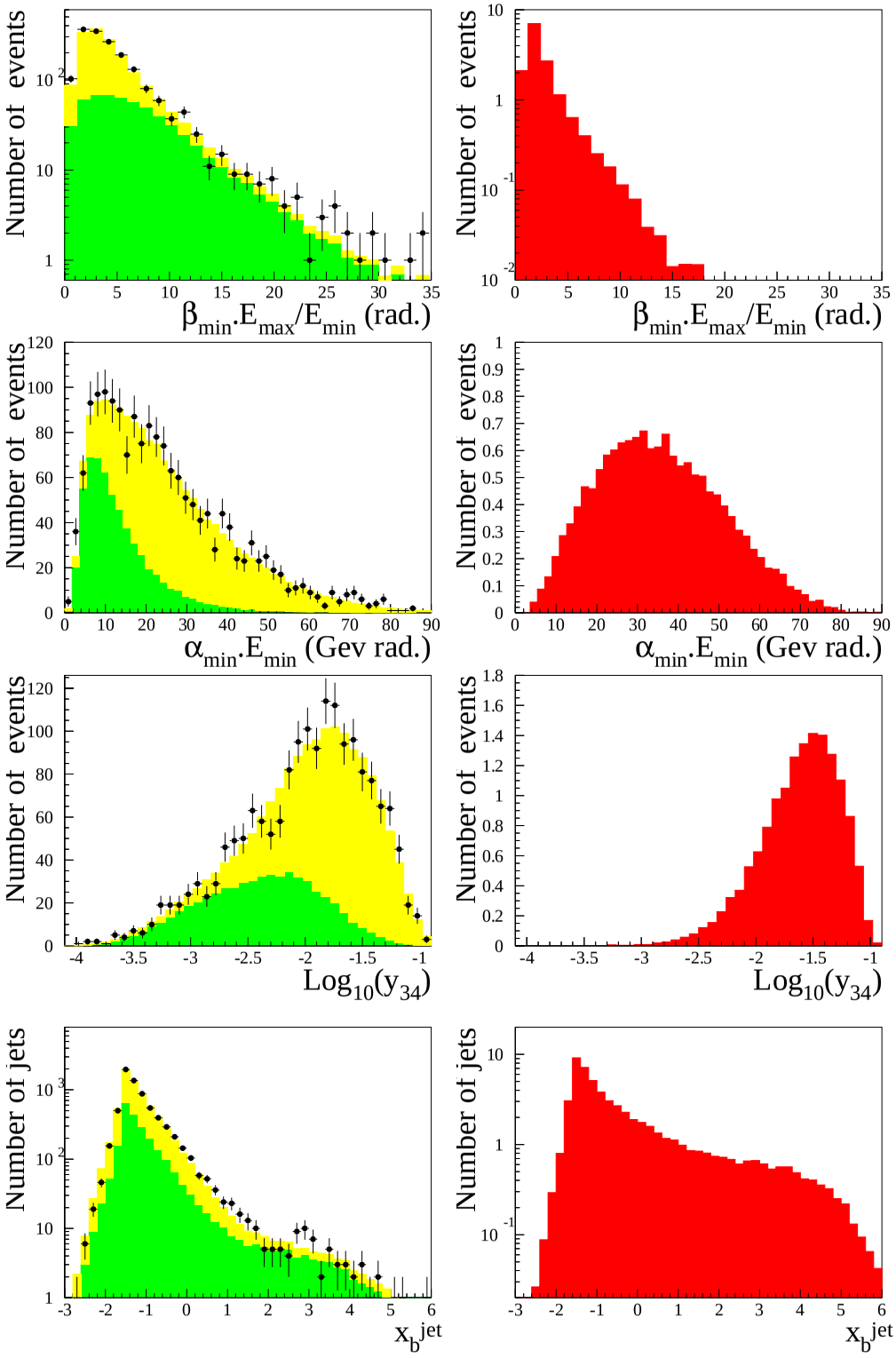

Figure 9: Hq$\bar{\text{q}}$ channel: *distributions of the main analysis variables at the preselection level. The points with error bars represent the data. The left hand side histograms show the different backgrounds and the right hand side ones show the expected signal distributions for* m_{H} *=95* GeV/c^2.

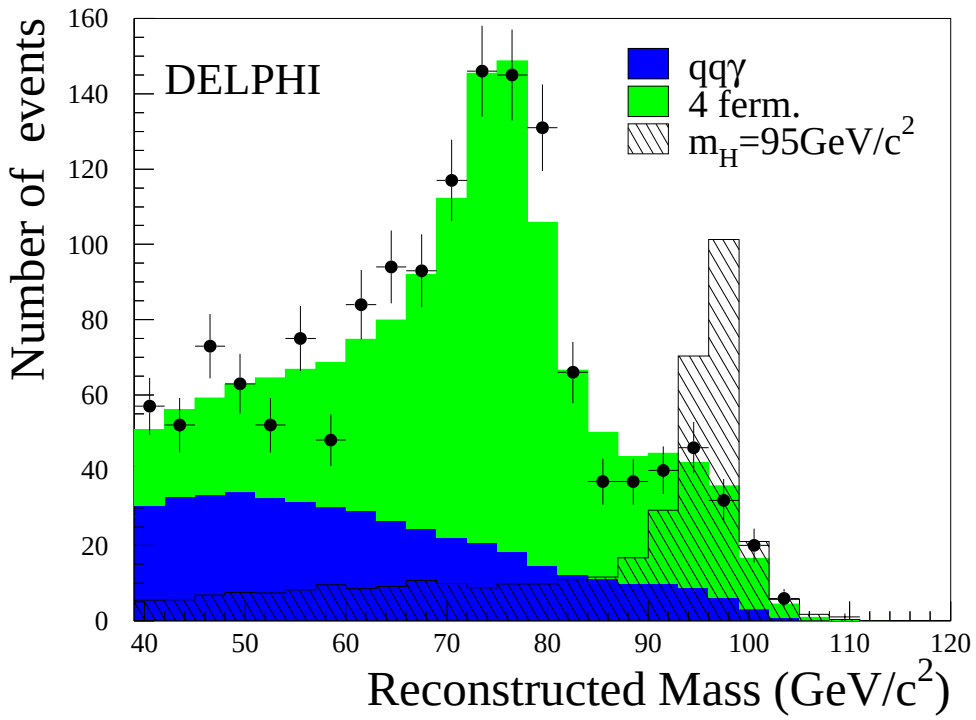

Figure 10: Hqq̄ channel: *The reconstructed mass at the preselection level. Note that the signal corresponds to* 400 *times the luminosity for clarity.*

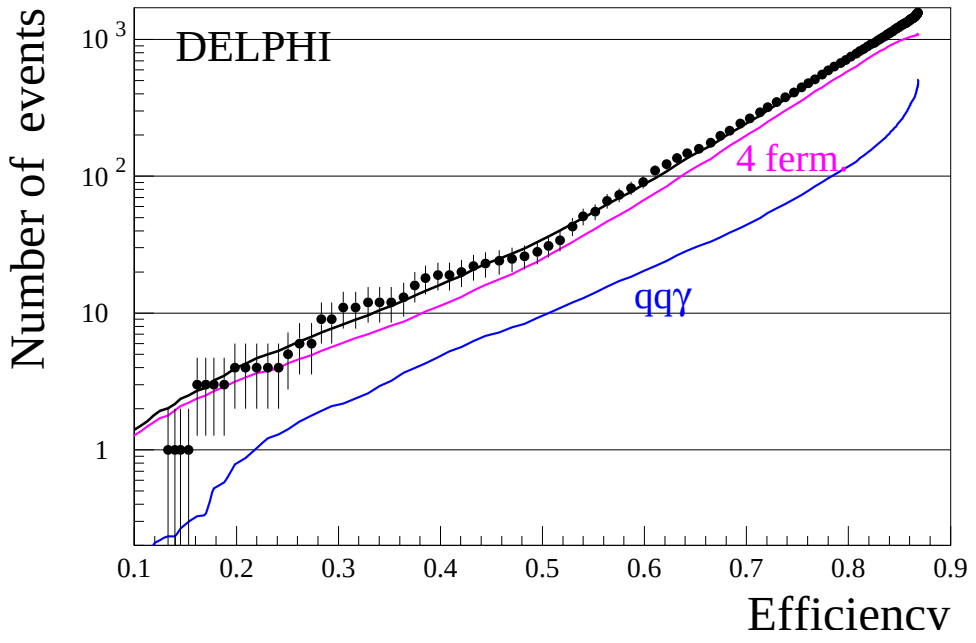

Figure 11: Hqq̄ channel: *Efficiency versus total background as a result of varying the cut on the Likelihood. The contribution of different backgrounds are shown separately. Points with error bars are the data and the upmost black line the total expected background.*

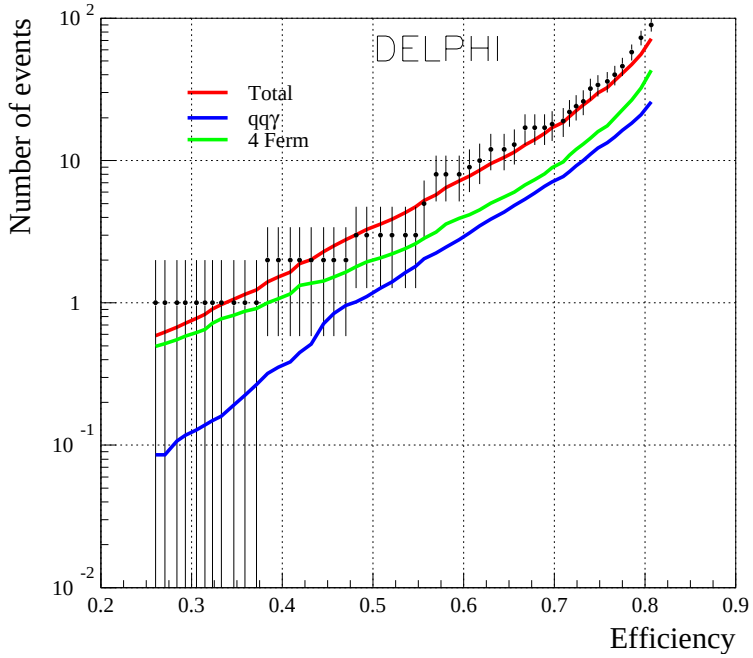

Figure 12: hA channel: *Efficiency versus total background as a result of varying the cut on the Likelihood. The contribution of different backgrounds are shown separately. Points with error bars are the data and the upmost black line the total expected background.*

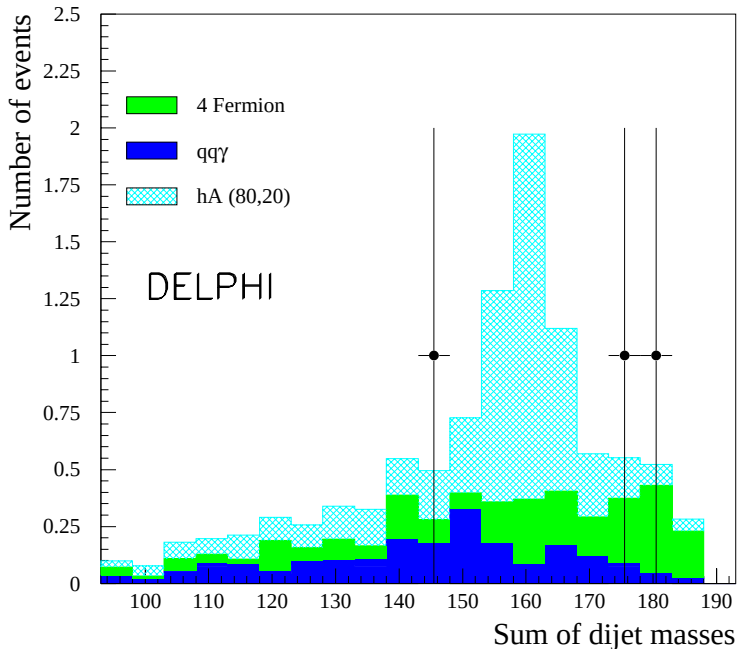

Figure 13: hA hadronic channel: *Mass distribution for the sum of the di-jets in data and MC at the end of the* hA *4-jet analysis at the 55% efficiency level. The signal, with* $m_{\mathrm{A}} = 80$ GeV/c^2 *and* $\tan\beta = 20$ *is normalised to the data.*

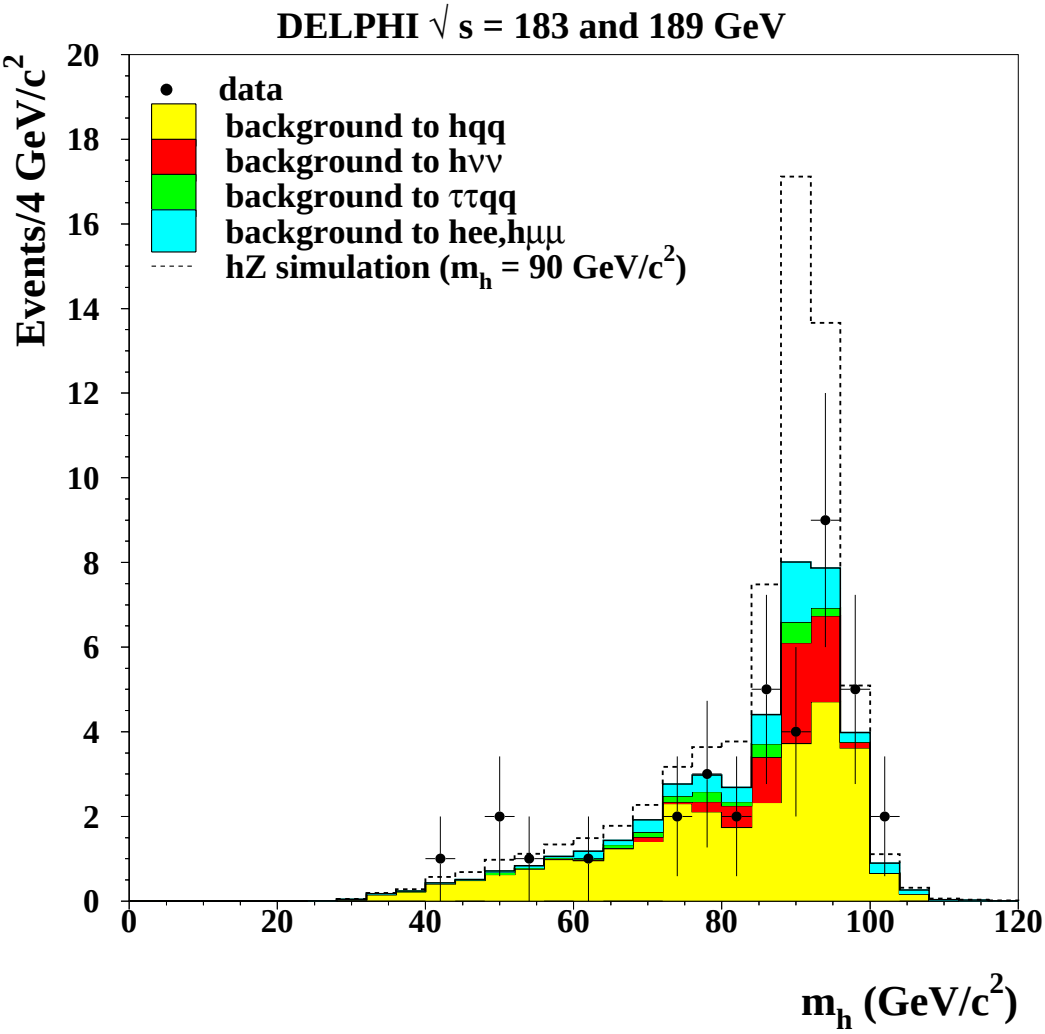

Figure 14: *Final distribution of the reconstructed Higgs boson mass when combining all* hZ *analyses at 182.7 and 188.7* GeV*. Data are compared with background expectations. The expected spectrum, with the correct rate, from a signal at 90* GeV/c^2 *is also shown added to the background contributions, as the dotted histogram.*

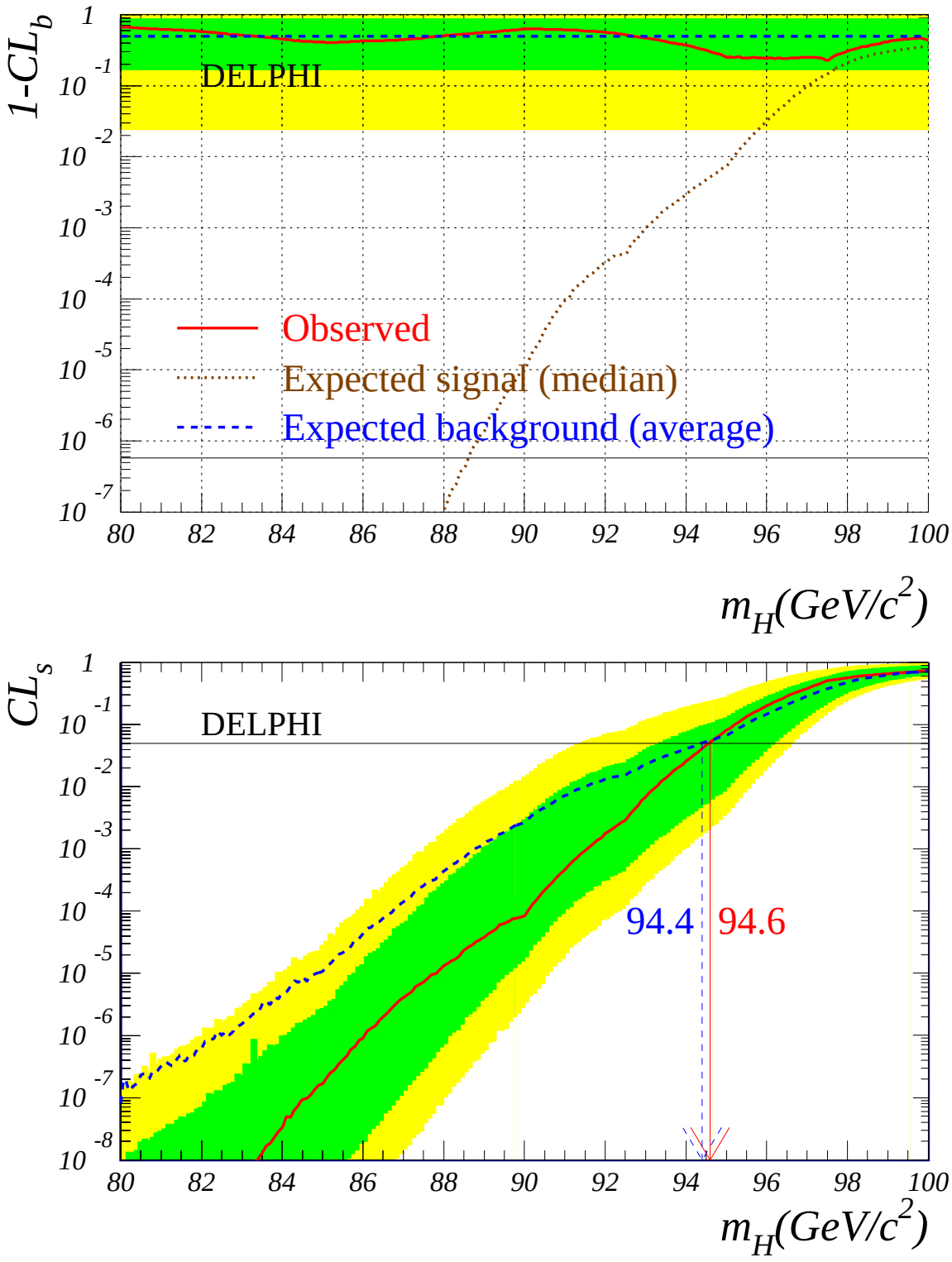

Figure 15: *Confidence levels as a function of the SM Higgs boson mass. Curves are shown for the expected (dashed) and observed (solid) confidences and the bands correspond to the 68.3% and 95% confidence intervals. Top: Confidence level in the background hypothesis. Bottom: Confidence level in the signal hypothesis. The intersections of the horizontal line at 5% with the curves define the expected and observed 95% CL lower limits on the Higgs boson mass.*

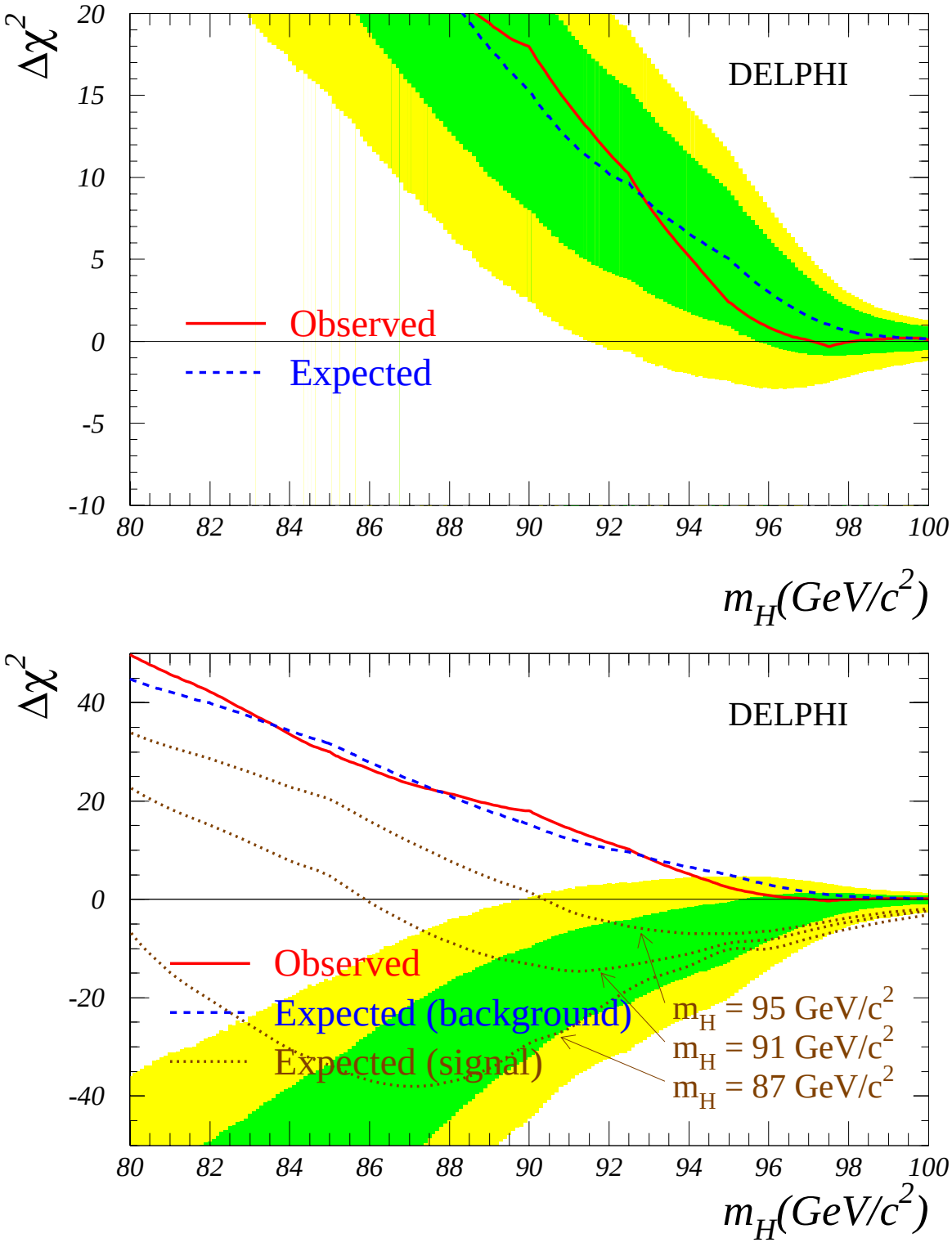

Figure 16: *The effective $\Delta\chi^2$ with which each SM Higgs mass is excluded (solid) and the expected value of the same (dashed). Top: Expectation in case of background only; the dark/light bands correspond to the 68.3% / 95% confidence intervals. Bottom: the bands represent the confidence intervals for the minima of the expectation curves in case of a signal (dotted lines).*

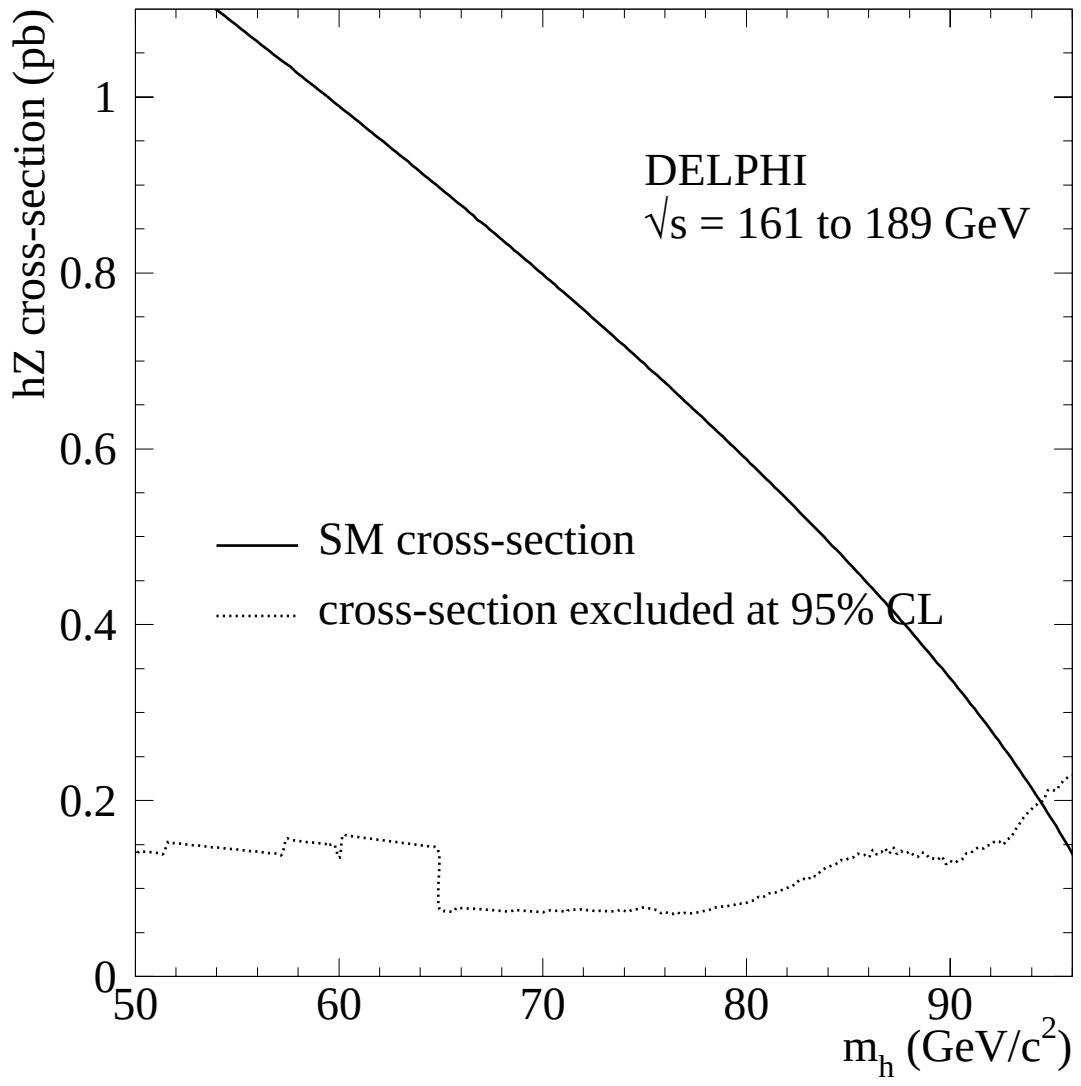

Figure 17: *95% CL excluded cross-sections as a function of the Higgs boson mass compared with the SM expectation.*

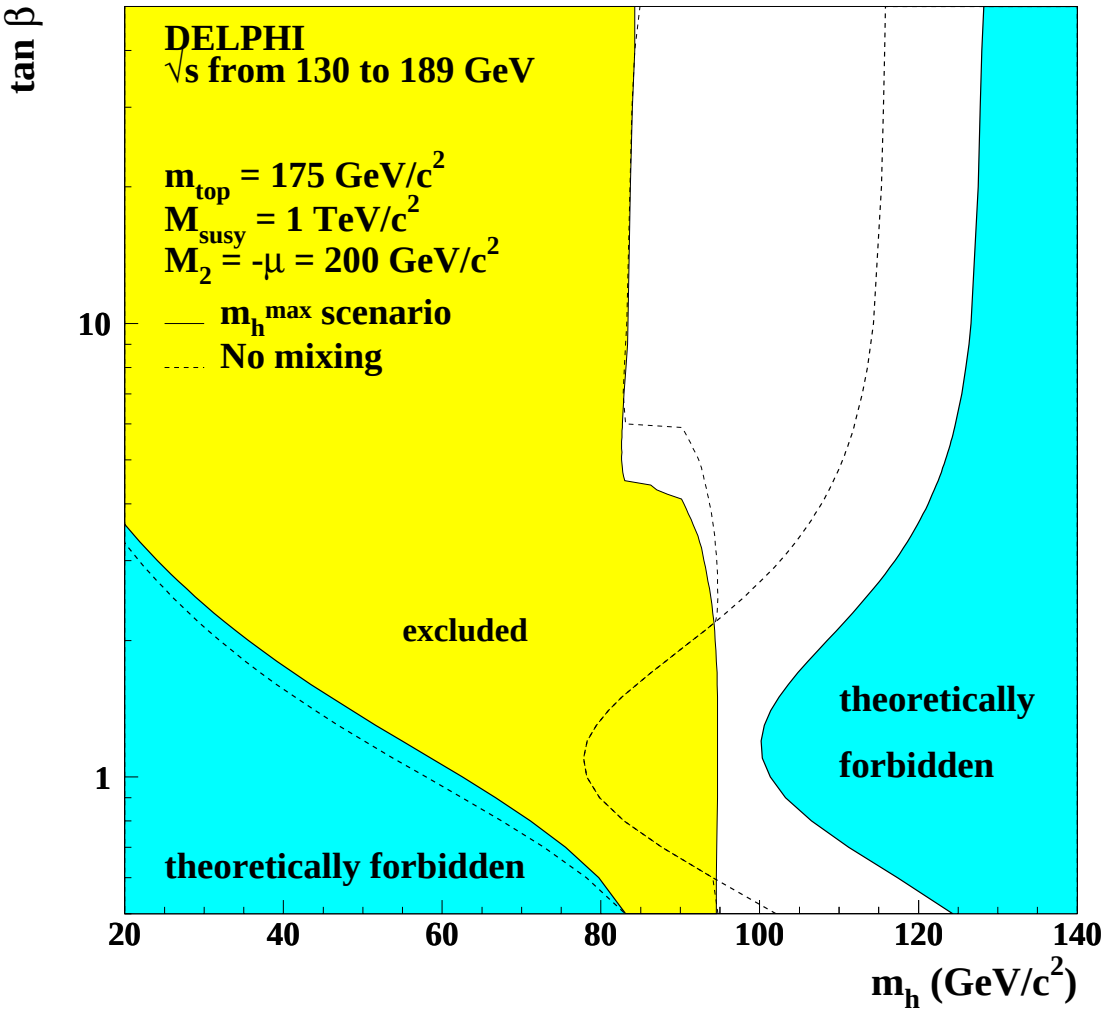

Figure 18: *Regions in the* $(m_{\mathrm{h}}, \tan\beta)$ *plane excluded at 95% CL by the searches in the* hZ *and* hA *channels up to* $\sqrt{s} = 189$ GeV. *Two extreme hypotheses for the mixing in the stop sector are considered. The regions not allowed by the MSSM model for* $m_{\mathrm{top}} = 175$ GeV/c^2, $M_{\mathrm{SUSY}} = 1$ TeV/c^2, $M_2 = -\mu = 200$ GeV/c^2 *and* $m_{\mathrm{A}} < 1$ MeV/c^2 *or* $m_{\mathrm{A}} > 1$ TeV/c^2 *are also indicated (shaded for the* m_{h}^{max} *scenario).*

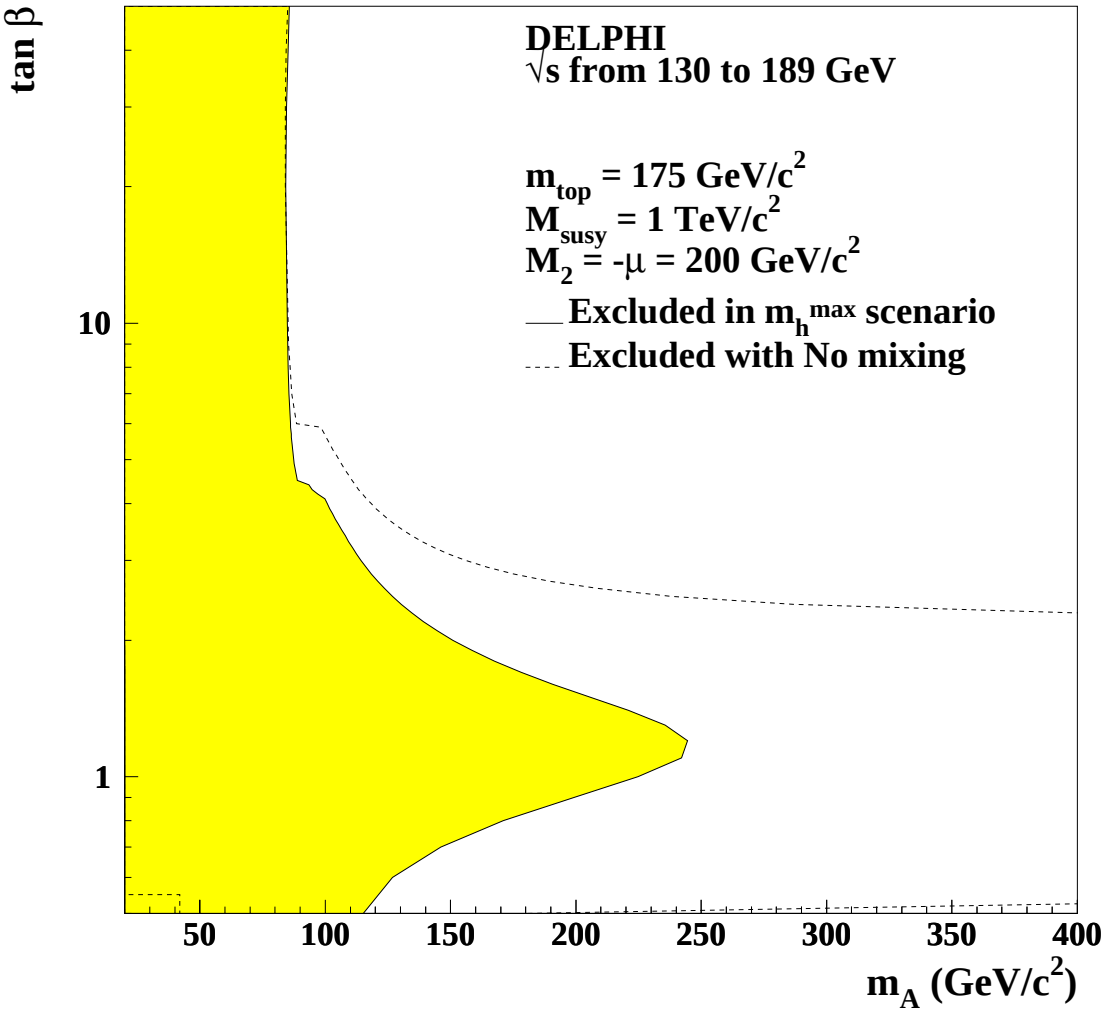

Figure 19: *Regions in the* (m_{A} , $\tan\beta$) *plane excluded at 95% CL by the searches in the* hZ *and* hA *channels up to* $\sqrt{s} = 189$ GeV. *Two extreme hypotheses for the mixing in the stop sector are presented.*

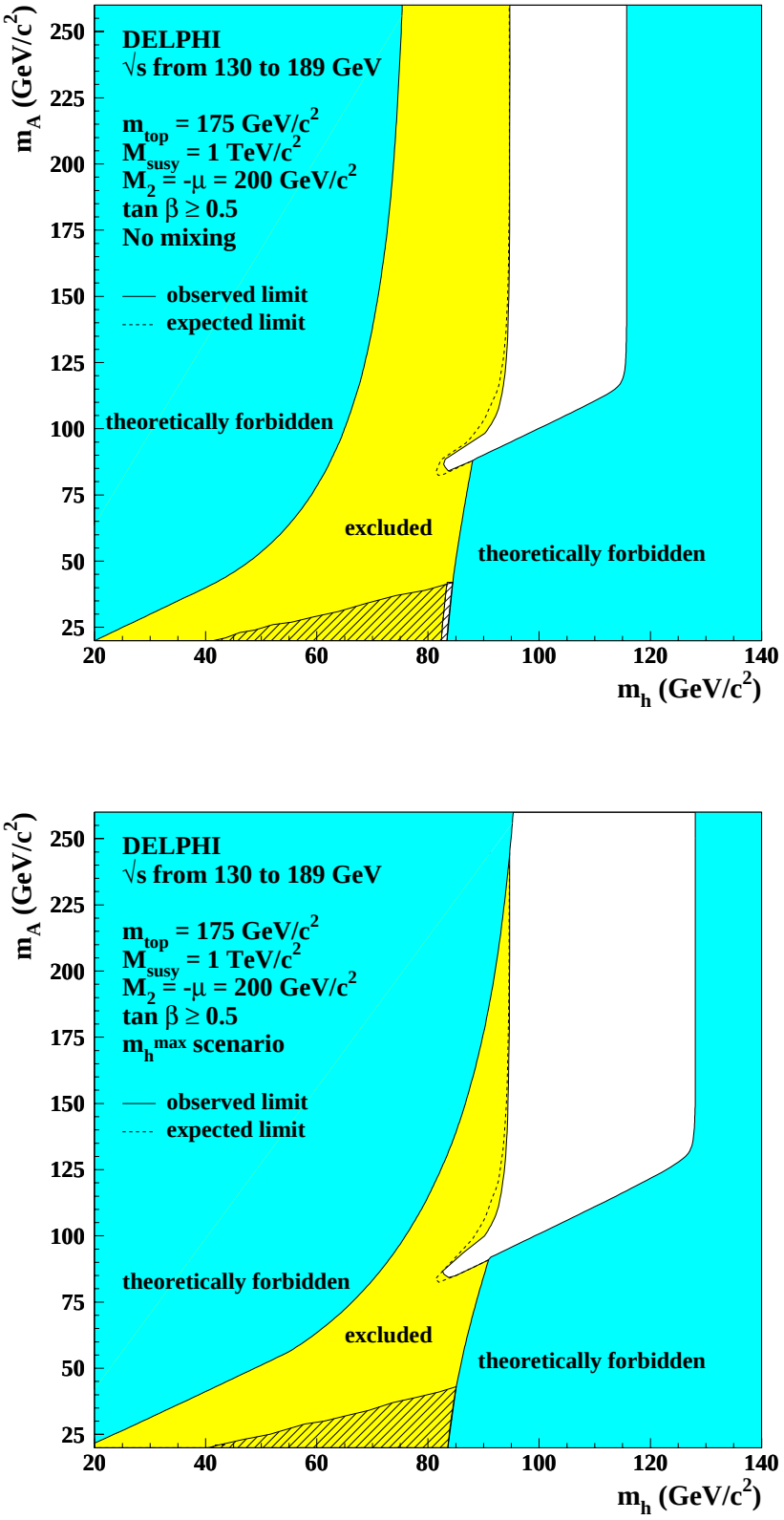

Figure 20: *Regions in the* $(m_{\mathrm{A}}, m_{\mathrm{h}})$ *plane excluded at 95% CL by the searches in the* hZ *and* hA *channels up to* $\sqrt{s} = 189$ GeV *(in light grey). Two extreme hypotheses for the mixing in the stop sector are presented. The regions not allowed by the MSSM model for* $m_{\mathrm{top}} = 175$ GeV/c^2, $M_{\mathrm{SUSY}} = 1$ TeV/c^2, $M_2 = -\mu = 200$ GeV/c^2 *and* $m_{\mathrm{A}} < 1$ MeV/c^2 *or* $m_{\mathrm{A}} > 1$ TeV/c^2 *are shaded. The hatched area shows the region where the* $\mathrm{h} \to \mathrm{AA}$ *decay occurs.*

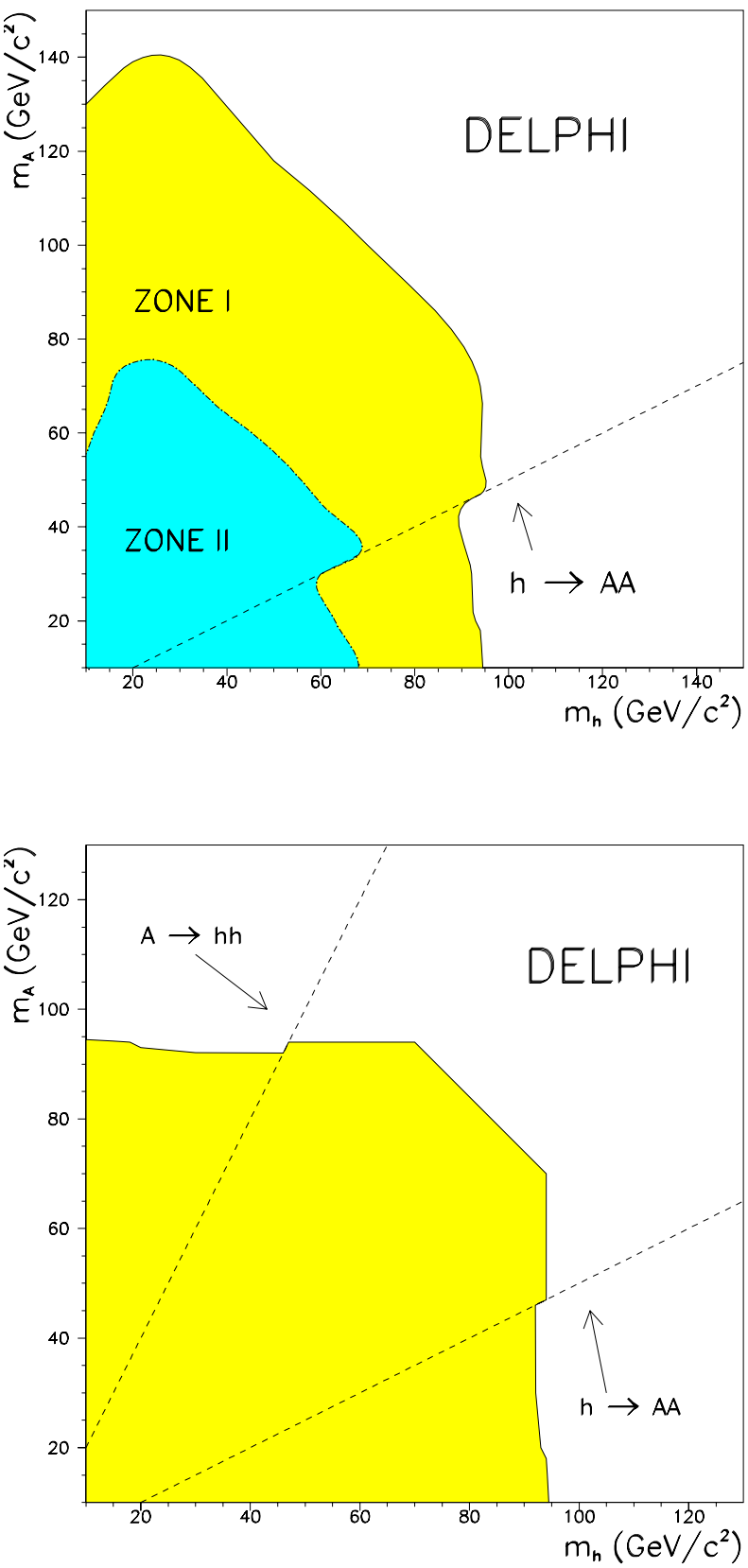

Figure 21: *Excluded regions at the 95% CL a) in the CP–conserving model (with dominant b–decays (*ZONE I*) and dominant non–b decays (*ZONE II*)) and b) in the CP–violating model.*